August 2023

# ANALYSIS OF NONEQUILIBRIUM LANGEVIN DYNAMICS FOR STEADY HOMOGENEOUS FLOWS

Abdel Kader A. Geraldo
*University of Massachusetts Amherst*

# ANALYSIS OF NONEQUILIBRIUM LANGEVIN DYNAMICS FOR STEADY HOMOGENEOUS FLOWS

A Dissertation Presented

by

ABDEL KADER A. GERALDO

Submitted to the Graduate School of the
University of Massachusetts Amherst in partial fulfillment
of the requirements for the degree of

DOCTOR OF PHILOSOPHY

May 2023

Department of Mathematics and Statistics

# ANALYSIS OF NONEQUILIBRIUM LANGEVIN DYNAMICS FOR STEADY HOMOGENEOUS FLOWS

A Dissertation Presented

by

ABDEL KADER A. GERALDO

Approved as to style and content by:

Matthew Dobson, Chair

Luc Rey-Bellet, Member

Hongkun Zhang, Member

Peng Bai, Department of Chemical Engineering, Member

Tom Braden, Graduate Program Director
Department of Mathematics and Statistics

# DEDICATION

*To my beloved family and friends*

# ACKNOWLEDGMENTS

I would like to express my sincere gratitude to Dr. Matthew Dobson, my advisor and committee chair, for his unwavering support and vital guidance throughout my entire academic journey at the University of Massachusetts. This incredible novel started with my participation in undergraduate research organized and sponsored by the department of Mathematics and Statistics. All milestones achieved since then would not have been possible without Dr. Matthew Dobson's expertise and unrelenting commitment.

I express my sincere gratitude to the remaining members of my committee, namely Dr. Luc Rey-Bellet, Dr. Hongkun Zhang, and Dr. Peng Bai, for their invaluable comments and feedback. In addition, I would like to extend my appreciation to Dr. Gabriel Stoltz for his valuable comments on the second chapter of this dissertation, the department's professors and staff members for their guidance, teaching, and consistent support throughout my scholastic path.

I would like to thank the department for financially supporting my research and presentation, and the Society for Industrial and Applied Mathematics to fund my trip and presentation at the 2022 SIAM Annual Meeting.

Furthermore, I would like to express my gratitude to my family for providing constant encouragement throughout this procedure. My deepest appreciation goes to my father, who has worked tirelessly day and night to support me and my siblings

and has sponsored our immigration to the United States. None of this would have been possible without him. I am grateful to my mother for her unending prayers and support. I am also thankful to my siblings who, above everything, have always been available when I needed them.

I owe my gratitude to Dr. Fioklou and his family for their countless advice and assistance. I am grateful to Renato for his friendship and availability when addressing project-related issues. I am grateful to all my friends who have made my university path easier through their friendship and help.

# ABSTRACT

## ANALYSIS OF NONEQUILIBRIUM LANGEVIN DYNAMICS FOR STEADY HOMOGENEOUS FLOWS

MAY 2023

ABDEL KADER A. GERALDO

B.S., UNIVERSITY OF MASSACHUSETTS AMHERST

M.S., UNIVERSITY OF MASSACHUSETTS AMHERST

Ph.D., UNIVERSITY OF MASSACHUSETTS AMHERST

Directed by: Professor Matthew Dobson

First, we propose using rotating periodic boundary conditions (PBCs) [13] to simulate nonequilibrium molecular dynamics (NEMD) in uniaxial or biaxial stretching flow. These specialized PBCs are required because the simulation box deforms with the flow. The method extends previous models with one or two lattice remappings and is simpler to implement than PBCs proposed by Dobson [10] and Hunt [24].

Then, using automorphism remapping PBC techniques such as Lees-Edwards for shear flow and Kraynik-Reinelt for planar elongational flow, we demonstrate exponential convergence to a steady-state limit cycle of incompressible two-dimensional NELD. To demonstrate convergence [12], we use a technique similar to [R. Joubaud,

G. A. Pavliotis, and G. Stoltz, 2014] after converting NELD to Lagrangian coordinates.

Finally, we propose a number of numerical schemes for solving Nonequilibrium Langevin Dynamics (NELD) [11], and we examine the strong rate of convergence for each scheme. Lees-Edwards and Kraynik-Reinelt boundary conditions, as well as their generalizations, are used in the schemes considered here. We demonstrate that when implementing standard stochastic integration schemes with these boundary conditions, care must be taken to avoid a breakdown in the strong order of convergence.

# TABLE OF CONTENTS

# LIST OF TABLES

**Table** **Page**

# LIST OF FIGURES

**Figure** **Page**

# INTRODUCTION

Nonequilibrium molecular dynamics (NEMD) [17, 62] techniques are one tool used to study molecular fluids under steady flow, and for instance, some recent applications can be found in [29, 48, 47, 44, 49, 45, 57, 40, 18, 36]. However, there are special challenges in formulating the periodic boundary conditions (PBCs) in the nonequilibrium setting [9, 64, 3, 59, 60].

In the molecular simulation we are considering, the particles have an average flow that is consistent with a homogeneous background flow matrix $A = \nabla \mathbf{u} \in \mathbb{R}^{3\times 3}$. This flow is used to simulate the micro-scale motion of a fluid with local strain rate $\nabla \mathbf{u}$. We represent the coordinates of the simulation box using three linearly independent vectors coming from the origin, and we write the vectors as the columns of the matrix

$$L_t = \begin{bmatrix} \mathbf{v}_t^1 & \mathbf{v}_t^2 & \mathbf{v}_t^3 \end{bmatrix} \in \mathbb{R}^{3\times 3}, \qquad t \in [0, \infty).$$

To be consistent with the background flow, a particle with coordinates $(\widetilde{\mathbf{q}}, \widetilde{\mathbf{p}})$, where $\widetilde{\mathbf{q}}$ is the position and $\widetilde{\mathbf{p}}$ is the momentum has images with coordinates $(\widetilde{\mathbf{q}} + L_t\mathbf{n}, \widetilde{\mathbf{p}} + AL_t\mathbf{n})$, where $\mathbf{n} \in \mathbb{Z}^3$ are triples of integers. Since the image momentum is the time derivative of its position, we have

$$\frac{d}{dt}(\widetilde{\mathbf{q}} + L_t\mathbf{n}) = \widetilde{\mathbf{p}} + AL_t\mathbf{n},$$

which implies that the simulation box deforms with the flow

$$\frac{d}{dt}L_t = AL_t.$$

The resulting lattice deformation

$$L_t = e^{At}L_0$$

can become degenerate and eventually lead to a particle and some of its images becoming arbitrarily close, if the initial lattice $L_0$ is not chosen carefully. We want to ensure that the minimum distance between a particle and its images is always greater than zero,

$$d = \inf_{\substack{\mathbf{n}\in\mathbb{Z}^3\setminus 0 \\ t\in\mathbb{R}\geq 0}} ||L_t\mathbf{n}||_2 > 0. \tag{1}$$

This is required in order to have long-term stable periodic boundary conditions for NEMD flows.

We consider a class of PBCs that are based on remapping the simulation box at different points during the simulation by selecting a new set of basis vectors for the lattice $L_t$ that describes the simulation box. This remapping is known as a lattice automorphism and can be represented as a $3 \times 3$ integer matrix with a determinant one. This was first used for shear flow by Lees-Edwards (LE) [31], and Kraynik

and Reinelt (KR) [28] extended it to planar elongational flow. Although these algorithms produce time-periodic remappings, KR demonstrated that using such matrices, a time-periodic remapping to the original simulation box is impossible for general three-dimensional flows. PBCs for general three-dimensional diagonalizable flow were developed by Dobson [10] and Hunt [24] using a similar remapping technique to the KR scheme. These schemes employ more than one automorphism matrix, resulting in a non-time periodic remapping. The first purpose of this project is to present an advantageous rotating box algorithm applicable to uniaxial stretching flow (USF) and biaxial stretching flow (BSF). Specifically, we will demonstrate that using the class of automorphism matrices with a pair of complex conjugate eigenvalues, we can construct a single remapping matrix algorithm that is time periodic up to a rotation matrix and has a larger minimum distance (1.1) than those of the GenKR and Hunt algorithms.

The NELD equation is derived in [38, 14] and it is expressed in terms of relative momentum $\widetilde{\mathbf{p}}$ as

$$\begin{cases} d\widetilde{\mathbf{q}} &= (\widetilde{\mathbf{p}} + A\widetilde{\mathbf{q}})dt, \\ d\widetilde{\mathbf{p}} &= -\nabla V(\widetilde{\mathbf{q}})dt - \gamma\widetilde{\mathbf{p}}dt + \sigma dW. \end{cases} \tag{2}$$

Here, $\sigma^2 = \frac{2\gamma}{\beta}$ denotes the fluctuation coefficient, $\beta$ is the inverse temperature, $V$ represents the potential, and its gradient is assumed to be finite. The particles coordinates domain is represented by $(\widetilde{\mathbf{q}}, \widetilde{\mathbf{p}}) \in \widetilde{\mathcal{L}}_t^d \times \mathbb{R}^{3d}$, where the set

$$\widetilde{\mathcal{L}}_t = \{L_t\mathbf{x} \;\big|\; \mathbf{x} \in \mathbb{T}^3\} \tag{3}$$

defines the time-dependent simulation box. It is worth noting that when there is no background flow, (2.1) becomes equilibrium Langevin Dynamics

$$\begin{cases} d\mathbf{q} &= \mathbf{p}dt, \\ d\mathbf{p} &= -\nabla V(\mathbf{q})dt - \gamma \mathbf{p}dt + \sigma dW, \end{cases}$$

with $(\mathbf{q}, \mathbf{p}) \in \mathcal{L}_0^d \times \mathbb{R}^{3d}$.

It has been proven (see for instance [56, 37, 7, 33, 34, 4]) that under suitable conditions, the equilibrium Langevin Dynamics is ergodic with respect to the Boltzmann-Gibbs distribution

$$\nu(\mathbf{q}, \mathbf{p})d\mathbf{q}d\mathbf{p} = \frac{1}{Z} e^{-\beta H(\mathbf{q},\mathbf{p})} d\mathbf{q}d\mathbf{p}, \quad Z = \int_{\mathcal{L}_0^d \times \mathbb{R}^{3d}} e^{-\beta H(\mathbf{q},\mathbf{p})} d\mathbf{q}d\mathbf{p},$$

where $Z$ is the normalization constant, and $H$ is the Hamiltonian of the system given by

$$H(\mathbf{q}, \mathbf{p}) = \frac{1}{2} \langle \mathbf{p}, \mathbf{p} \rangle + V(\mathbf{q}).$$

However, convergence to a limiting measure for NELD in moving domains has not been established. The project's second objective is to establish the existence, uniqueness, and exponential convergence of NELD to a limit cycle in moving domains, building upon the work presented in [26].

In the final stage of this project, we examine the strong convergence properties of commonly used stochastic integrators in NELD simulations. The strong convergence

is an essential tool to consider as it guarantees the accuracy of the dynamical trajectories obtained in the simulations. We will specifically focus on how the periodic boundary conditions affect the convergence of the proposed integrators.

From a sampling standpoint, it is more common to look at the sampling bias due to errors of the invariant measure for the integrator; however, unlike the equilibrium Langevin case, the invariant measure for NELD with deforming boundary conditions is not known analytically. Our approach will involve adapting the standard method of computing the truncation error through Ito-Taylor expansions, as outlined in sources such as [27, 53], to the non-equilibrium case. The unique property of our analysis is the examination of how the stochastic integrators interact with the remapping of the simulation box, which is a result of the use of periodic boundary conditions. We show that when certain standard schemes are implemented naively, they can exhibit a breakdown in convergence, and we develop alternative methods to overcome this problem. The Ito-Taylor expansion will be used to calculate the order of convergence, and several standard first and second-order schemes will be numerically and theoretically evaluated.

# CHAPTER 1

# SIMPLE PERIODIC BOUNDARY CONDITIONS FOR MOLECULAR SIMULATION OF UNIAXIAL FLOW

**Note.** This chapter is published and cited as: *"Simple periodic boundary conditions for molecular simulation of uniaxial flow" by Matthew Dobson and Abdel Kader A. Geraldo in 2023 Journal of Computational Physics 473 , pp. 111740, doi.org/10.1016/j.jcp.2022.111740*

## 1.1 Abstract

We present rotating periodic boundary conditions (PBCs) for the simulation of nonequilibrium molecular dynamics (NEMD) under uniaxial stretching flow (USF) or biaxial stretching flow (BSF). Such nonequilibrium flows need specialized PBCs since the simulation box deforms with the background flow. The technique builds on previous models using one or two lattice remappings, and is simpler than the PBCs developed for the general three dimensional flow. For general three dimensional flows, Dobson [10] and Hunt [24] proposed schemes which are not time-periodic since they use more than one automorphism remapping. This paper presents a single automorphism remapping PBCs for USF and BSF which is time periodic up to a rotation matrix and has better minimum lattice spacing properties.

## 1.2 Introduction

Nonequilibrium molecular dynamics (NEMD) [17, 62] techniques are one tool used to study molecular fluids under steady flow, and some recent applications can be found in [29, 48, 47, 44, 49, 45, 57, 40, 18, 36]. However, there are special challenges in formulating the periodic boundary conditions (PBCs) in the nonequilibrium setting [9, 64, 3, 59, 60].

We consider a molecular simulation where the particles have an average flow consistent with a homogeneous background flow matrix $A = \nabla \mathbf{u} \in \mathbb{R}^{3\times 3}$. This flow is used to simulate the micro-scale motion of a fluid with local strain rate $\nabla \mathbf{u}$. We denote the coordinates of the simulation box via three linearly independent vectors coming from the origin, and we write the vectors as the columns of the matrix

$$L_t = \begin{bmatrix} \mathbf{v}_t^1 & \mathbf{v}_t^2 & \mathbf{v}_t^3 \end{bmatrix} \in \mathbb{R}^{3\times 3}, \qquad t \in [0, \infty).$$

To be consistent with the background flow, a particle with coordinates $(\widetilde{\mathbf{q}}, \widetilde{\mathbf{p}})$, where $\widetilde{\mathbf{q}}$ is the position and $\widetilde{\mathbf{p}}$ is the velocity, has images with coordinates $(\widetilde{\mathbf{q}} + L_t\mathbf{n},\ \mathbf{v} + AL_t\mathbf{n})$, where $\mathbf{n} \in \mathbb{Z}^3$ are triples of integers. Since the image velocity is the time derivative of its position we have

$$\frac{d}{dt}(\widetilde{\mathbf{q}} + L_t\mathbf{n}) = \ \mathbf{v} + AL_t\mathbf{n},$$

which implies that the simulation box deforms with the flow

$$\frac{d}{dt}L_t = AL_t.$$

If the initial lattice $L_0$ is not chosen carefully, the resulting lattice deformation

$$L_t = e^{At} L_0$$

can become degenerate and lead to a particle and some of its images becoming arbitrarily close. We want to ensure that the minimum distance between a particle and its images is bounded away from zero for all time,

$$d = \inf_{\substack{\mathbf{n}\in\mathbb{Z}^3\setminus 0 \\ t\in\mathbb{R}_{\geq 0}}} ||L_t\mathbf{n}||_2 > 0. \tag{1.1}$$

This is necessary in order to have long-time stable periodic boundary conditions for NEMD flows.

We consider a class of PBCs based on remapping the simulation box at various times during the simulation by choosing a new set of basis vectors for the lattice $L_t$ that describes the simulation box. This remapping is called a lattice automorphism and can be represented as a $3 \times 3$ integer matrix with determinant one. This was first used for the case of shear flow by Lees-Edwards [31] and was then extended to the case of planar elongational flow by Kraynik and Reinelt (KR) [28]. Those algorithms result in remappings which are periodic in time, though KR showed that a time-periodic remapping to the original simulation box using such matrices is impossible for general three dimensional flows. Dobson [10] and Hunt [24] developed PBCs for general three dimensional diagonalizable flow using similar remapping technique to

the KR scheme. Those schemes use more than one automorphism matrix and result in a remapping that is not time periodic. In this paper we present a rotating box algorithm applicable to uniaxial stretching flow (USF) and biaxial stretching flow (BSF) which features advantageous properties. Namely, we will show that using the class of automorphism matrices that have a pair of complex conjugate eigenvalues, we can construct a single remapping matrix algorithm which is time periodic up to a rotation matrix and whose minimum distance (1.1) is larger than those of the GenKR and Hunt algorithms.

The outline of this paper is as follows. Section 1.3 gives the background for nonequilibrium PBCs, particularly, shear flow, planar elongational flow, and incompressible, diagonalizable three dimensional flows. Section 1.4 presents the rotating box algorithm, and Section 1.5 gives the prove that the deformed lattice obtained is not time periodic. Section 1.6 compares the rotating box algorithm with the existing three dimensional flow PBCs.

## 1.3 Background

In this section, we give a description of the existing remapping PBCs, starting with shear flow and planar elongational flow. In the case of three dimensional flows, the generalized KR (GenKR) algorithm developed by Dobson and Hunt is presented. All the algorithms follow the same procedure: given a background flow $A$, for each time $t$ we find the appropriate integer power of the chosen automorphism matrix (or matrices) to remap the lattice $L_t$.

### 1.3.1 Shear Flow

We first consider the shear flow case where the background matrix $A$ is given by

$$A = \begin{bmatrix} 0 & \epsilon & 0 \\ 0 & 0 & 0 \\ 0 & 0 & 0 \end{bmatrix}.$$

At time $t$, the lattice is given by

$$L_t = \begin{bmatrix} 1 & t\epsilon & 0 \\ 0 & 1 & 0 \\ 0 & 0 & 1 \end{bmatrix} L_0 \text{ where } L_0 = \begin{bmatrix} 1 & 0 & 0 \\ 0 & 1 & 0 \\ 0 & 0 & 1 \end{bmatrix}.$$

A highly sheared box makes the computation of interparticle interactions more difficult, however this problem can be overcome by looking at the geometry of shears that are integer multiples of the box length. The Lees-Edwards (LE) boundary conditions [31] are used to prevent the simulation box from becoming too deformed. Whenever the simulation time is an integer multiple of the inverse shear rate, $t_n = n\epsilon^{-1}$, the simulation box is sheared by $n$ box lengths. We remap the simulation box with the matrix

$$M^n = \begin{bmatrix} 1 & -1 & 0 \\ 0 & 1 & 0 \\ 0 & 0 & 1 \end{bmatrix}^n = \begin{bmatrix} 1 & -n & 0 \\ 0 & 1 & 0 \\ 0 & 0 & 1 \end{bmatrix}, \quad n \in \mathbb{Z}$$

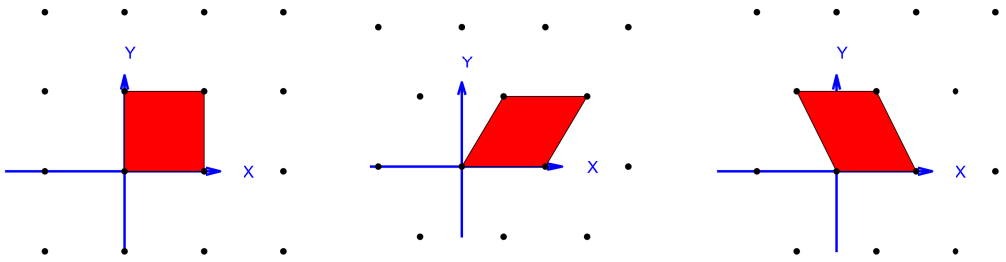


**Figure 1.1:** Remapping under shear flow. (Left) The initial configuration has its unit cell aligned with the coordinate axes. (Center) The unit cell deforms with the flow until a 45 degree angle, this is the configuration immediately before remapping. (Right) The unit cell after remapping. Note that the lattice is preserved by the remapping.

such that at a time $t$, the simulation box lattice is

$$L_t M^n = \begin{bmatrix} 1 & t\epsilon - n & 0 \\ 0 & 1 & 0 \\ 0 & 0 & 1 \end{bmatrix}, n \in \mathbb{Z}.$$

Since $M$ is an integer matrix with determinant equal to one, that is, $M \in SL(3, \mathbb{Z})$, the matrices $L_t$ and $L_t M^n$ generate the same lattice. Throughout the simulation, we choose $n = -\lfloor t\epsilon \rceil$ so that the stretch is at most half of the simulation box, and that this remapping process is time-periodic with period $t^* = \frac{1}{\epsilon}$, where $\lfloor x \rceil$ denotes $x$ rounded to nearest integer.

### 1.3.2 Planar Elongational Flow

Here, the background flow matrix is

$$A = \begin{bmatrix} \epsilon & 0 & 0 \\ 0 & -\epsilon & 0 \\ 0 & 0 & 0 \end{bmatrix},$$

meaning that the simulation box elongates in the $x$ direction and shrinks in the $y$ direction of the standard coordinate plane. To treat this case, KR proposed to remap the simulation box using a diagonalizable automorphism matrix $M \in SL(3, \mathbb{Z})$ that has the form

$$MV = V\Lambda, \quad \Lambda = \begin{bmatrix} \lambda & 0 & 0 \\ 0 & \lambda^{-1} & 0 \\ 0 & 0 & 1 \end{bmatrix}, \quad \lambda > 0, \quad \lambda \neq 1,$$

where $V$ denotes a matrix of eigenvectors of $M$. We consider the initial lattice $L_0 = V^{-1}$ so that at time $t$ when we apply $M^n$ to the lattice basis vectors

$$L_t M^n = e^{tA} L_0 M^n = e^{t\epsilon D} \Lambda^n V^{-1} = e^{A_t} V^{-1}, \text{ where } D = \begin{bmatrix} 1 & 0 & 0 \\ 0 & -1 & 0 \\ 0 & 0 & 0 \end{bmatrix},$$

and $A_t = (t\epsilon + n\log(\lambda))D$. Letting $n = -\left\lfloor t\frac{\epsilon}{\log(\lambda)} \right\rfloor$, the stretch of the flow $A_t$ remains bounded during the simulation, and in addition, it is time periodic with period $t_* = \frac{\log(\lambda)}{\epsilon}$. For instance,

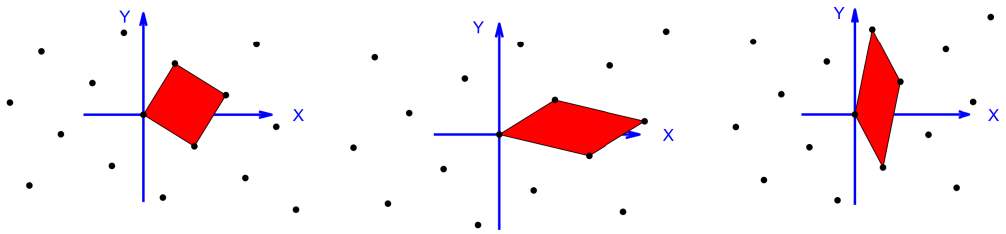


**Figure 1.2:** Remapping under planar elongational flow flow. (Left) The initial configuration of the unit cell is rotated with respect to the axes. (Center) The unit cell deforms with the flow, stretching in the x direction and compressing in the y direction. (Right) The unit cell after remapping, which preserves the lattice.

$$M = \begin{bmatrix} 2 & -1 & 0 \\ -1 & 1 & 0 \\ 0 & 0 & 1 \end{bmatrix}$$

is an example of matrix which gives a good minimum distance between a particle and its images.

For a 3D incompressible, diagonalizable flow

$$A = \begin{bmatrix} \epsilon_1 & 0 & 0 \\ 0 & \epsilon_2 & 0 \\ 0 & 0 & -\epsilon_1 - \epsilon_2 \end{bmatrix},$$

Dobson and Hunt proposed equivalent algorithms to control the deformation.

#### 1.3.2.1 Dobson's Approach

In [10], the author develops PBCs which use two commutative automorphism matrices $M_1, M_2 \in SL(3, \mathbb{Z})$ which have positive eigenvalues for the remapping of

the simulation box. Since the matrices are commutative, they are simultaneously diagonalizable, $M_i V = V\Lambda_i$, where $V$ denotes a matrix of the eigenvectors of $M_i$, and $\Lambda_i$ denotes the corresponding matrix of the eigenvalues. An example pair of commuting automorphism matrices is

$$M_1 = \begin{bmatrix} 1 & 1 & 1 \\ 1 & 2 & 2 \\ 1 & 2 & 3 \end{bmatrix} \quad \text{and } M_2 = \begin{bmatrix} 2 & -2 & 1 \\ -2 & 3 & -1 \\ 1 & -1 & 1 \end{bmatrix}.$$

The algorithm requires that the diagonal elements of the logarithm of the eigenvalue matrices $\hat{\omega}_i = \log(\Lambda_i)$ must be linearly independent, thus there exists $\delta_i \in \mathbb{R}$ solving $A = \delta_1\hat{\omega}_1 + \delta_2\hat{\omega}_2$. Now by considering the initial lattice $L_0 = V^{-1}$ and picking $n_i = -\lfloor t\delta_i \rceil$, we remark that the remapping of the simulation box with $M_1^{n_1} M_2^{n_2}$ results in the remapped lattice

$$\tilde{L}_t = L_t M_1^{n_1} M_2^{n_2} = e^{At} L_0 M_1^{n_1} M_2^{n_2} = e^{tA} \Lambda_1^{n_1} \Lambda_2^{n_2} V^{-1} = e^{A_t} V^{-1},$$

where the remaining stretch matrix

$$A_t = tA + n_1\hat{\omega}_1 + n_2\hat{\omega}_2 = (t\delta_1 - \lfloor t\delta_1 \rceil)\hat{\omega}_1 + (t\delta_2 - \lfloor t\delta_2 \rceil)\hat{\omega}_2,$$

is clearly bounded for every time $t$. Thus the minimum distance of the remapped lattice is bounded away from zero during the entire simulation.

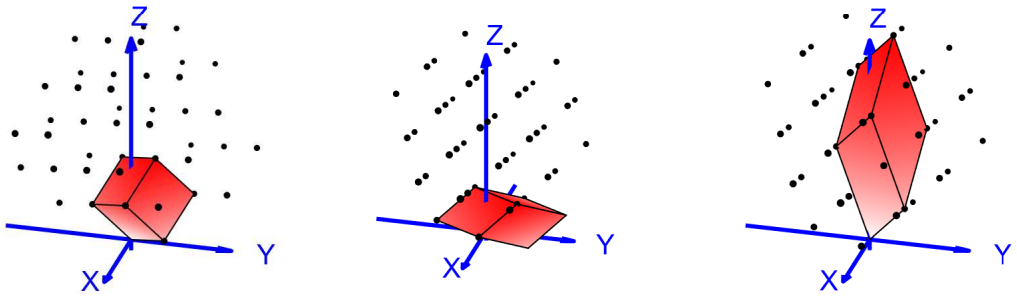


**Figure 1.3:** Remapping a biaxial stretching flow using the GenKR algorithm. (Left) The initial configuration of the unit cell, which is rotated with respect to the axes. (Center) The unit cell deforms with the flow, stretching in the x and y directions and compressing in the z direction. (Right) The unit cell after remapping, which preserves the lattice. The new cell is very tall and has room to compress further in the z direction.

#### 1.3.2.2 Hunt's Approach

Hunt's approach is similar to Dobson's, using the Lenstra-Lenstra-Lovász ( $LLL$) [35] transformation in place of a second automorphism matrix. As convention in this paper, we will describe Hunt's algorithm using column vectors instead of the row vectors used in the original paper. In fact, Hunt's PBCs consists of remapping the simulation box with the automorphism

$$M = \begin{bmatrix} 0 & 0 & 1 \\ 1 & 0 & -5 \\ 0 & 1 & 6 \end{bmatrix}, \text{ where } MV = V\Lambda$$

and choosing the initial lattice basis $L_0 = V^{-1}$. After applying $M^n$, the remapped lattice becomes

$$\tilde{L}_t = e^{tA} L_0 M_1^n = e^{tA} \Lambda_1^n V^{-1} = e^{A_t} V^{-1},$$

where $A_t = tA + n \log(\Lambda_1)$. This single matrix is not enough to control the deformation. The $LLL$ reduction algorithm [35] is used to reduce the remapped lattice $\tilde{L}_t$ by finding a matrix $\tilde{M} \in SL(3, \mathbb{Z})$ using a high precision reduction,

$$\hat{L}_t = LLL(\tilde{L}_t) = e^{A_t} V^{-1} \tilde{M}.$$

Unlike the GenKR approach, the matrix $\tilde{M}$ is solved for at each step. On this point, we can slightly improve the efficiency of Hunt's formulation by finding a commutative matrix $M_2$ manually and applying the GenKR approach to produce a remapped lattice whose minimum distance is close to optimal before the $LLL$ reduction step. The combination of these algorithms is presented as Algorithm 2, which is given in Section 1.6.

## 1.4 Rotating Box Algorithm

In this section, we will develop PBCs for USF and BSF that are time periodic up to a rotation. We write the background flow as

$$A = \epsilon D, \quad \text{where } D = \begin{bmatrix} 1 & 0 & 0 \\ 0 & 1 & 0 \\ 0 & 0 & -2 \end{bmatrix}.$$

Here, rather than choosing a pair of matrices $M_i \in SL(3,\mathbb{Z})$ with real spectrum, we will use a single matrix $M \in SL(3,\mathbb{Z})$ which has a pair of complex conjugate eigenvalues and use it to remap the simulation box.

Let us consider $M \in SL(3,\mathbb{Z})$, a matrix that has a pair of complex conjugate eigenvalues and write its real Jordan form

$$MV = V\Lambda \text{ where } \Lambda = \begin{bmatrix} \tilde{\eta} & -\tilde{\beta} & 0 \\ \tilde{\beta} & \tilde{\eta} & 0 \\ 0 & 0 & (\tilde{\eta}^2 + \tilde{\beta}^2)^{-1} \end{bmatrix},$$

where $\tilde{\eta}, \tilde{\beta} \neq 0$ , and $\tilde{\eta}^2 + \tilde{\beta}^2 \neq 1$ in order to avoid a full rotation. Taking the logarithm of $\Lambda$, we have

$$\log(\Lambda) = \begin{bmatrix} \eta & -\beta & 0 \\ \beta & \eta & 0 \\ 0 & 0 & -2\eta \end{bmatrix}, \text{ where } \eta = \frac{1}{2}\log(\tilde{\eta}^2 + \tilde{\beta}^2), \beta = \arctan\left(\frac{\tilde{\beta}}{\tilde{\eta}}\right),$$

which can be decomposed as:

$$\log(\Lambda) = \beta B + \eta D, \text{ where } B = \begin{bmatrix} 0 & -1 & 0 \\ 1 & 0 & 0 \\ 0 & 0 & 0 \end{bmatrix}.$$

For all time $t$, by choosing the initial lattice $L_0 = V^{-1}$, we can keep the lattice $L_t = e^{At}L_0$ bounded by remapping the simulation box with $M^n$

$$\tilde{L}_t = e^{At} L_0 M^n = e^{\epsilon D t} \Lambda^n V^{-1} = e^{n\beta B} e^{A_t} V^{-1},$$

where $A_t = \left(\epsilon t - \left\lfloor \frac{t\epsilon}{\eta} \right\rceil \eta\right) D$ for $n = -\left\lfloor \frac{t\epsilon}{\eta} \right\rceil$. We have already seen in the planar elongational flow case (Section 1.3.2) that the remapped lattice $e^{A_t} V^{-1}$ is bounded and time-periodic of period $t_* = \frac{\eta}{\epsilon}$. In this case, the remapped lattice is time-periodic up to the rotation matrix $R = e^{n\beta B}$. For a forward simulation in time, the algorithm reads

**Algorithm 1** R-KR

$V, \Lambda = RealJordan(M)$ ▷ Compute eigenbasis $V$ and the Jordan $\Lambda$ of $M$
$\eta D = \text{diag}(\log(\Lambda))$ ▷ Compute the diagonal part of the logarithm of $\Lambda$
$B = \log(\Lambda) - \eta D$ ▷ Compute the rotation part of logarithm of $\Lambda$
$L_0 = V^{-1}$ ▷ Compute the initial lattice

$\theta = 0$ ▷ Initialize $\theta$
**for** $i = 1 \ldots$ Nsteps **do**
  $n \leftarrow -\left\lfloor \frac{\theta}{\eta} + \tau \right\rceil$ ▷ Compute the power $n$ of $M$ necessary for the remap
  $\theta \leftarrow \theta + \tau\eta + \eta n$ ▷ Compute the remaining stretch value
  $\tilde{L} \leftarrow e^{n\beta B} e^{\theta D} V^{-1}$ ▷ Compute the lattice value at the $t$ iteration

Since the rotation matrix is bounded, we observe that the remapped unit cell is bounded during the simulation. In the next section, we show that the rotating algorithm is not time periodic using the fact that the rotation matrix is never equal to the identity matrix for any automorphism chosen.

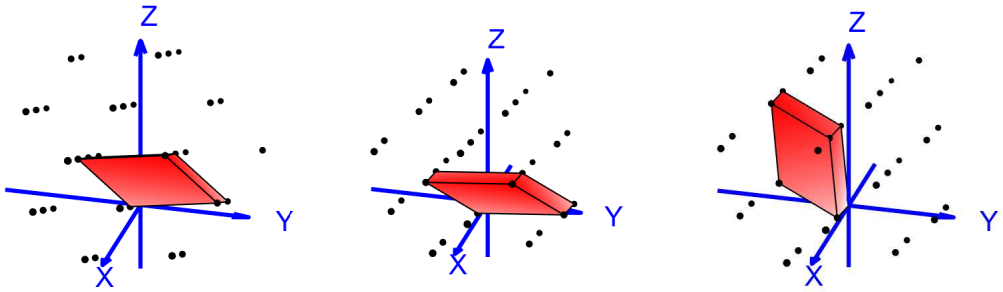


**Figure 1.4:** Remapping a biaxial stretching flow using the rotating box algorithm. (Left) The initial configuration of the unit cell, which is not a cube nor is it aligned with respect to the axes. (Center) The unit cell deforms with the flow, stretching in the x and y directions and compressing in the z direction. (Right) The unit cell after remapping, which preserves the lattice. Note that the center and rightmost figures are not related by a rotation, rather a full period results in a rotation from initial lattice to a new lattice.

## 1.5 Non time periodicity of the lattice in the rotating box algorithm

As mentioned above, for the class of automorphism matrices with real eigenvalues, it has been shown in [28] that it is impossible to construct KR PBCs with a time periodic lattice for USF or BSF. In this section, we will extend this demonstration to the class of automorphism matrices which have complex conjugate eigenvalues. Namely, we show in the following corollary that although the rotating box algorithm applied to USF or BSF is time-periodic up to a rotation matrix, there is no choice of $M \in SL(3,\mathbb{Z})$ where the period of the remapping aligns with that of the rotation. In other words, we show that rotation matrix $e^{n\beta B}$ is not equal to the identity matrix for $n \neq 0$, or equivalently $\beta$ is not a equal of $\pi$ times a rational number

$$\beta = \tan^{-1}\left(\frac{\tilde{\beta}}{\tilde{\eta}}\right) \neq 2\pi\frac{m}{n}, \quad n, m \in \mathbb{Z}, \quad n \neq 0,$$

for any $M$ considered in Section 1.4, i.e with complex eigenvalues one of the eigenvalue of $M$ is not equal to 1.

We start by recalling that $\tilde{\eta} \pm \mathrm{i}\tilde{\beta}, (\tilde{\eta}^2 + \tilde{\beta}^2)^{-1}$ are the roots of the characteristic polynomial $P(\lambda) = \lambda^3 - h\lambda^2 + k\lambda - 1, h, k \in \mathbb{Z}$ of $M \in SL(3, \mathbb{Z})$, and write these roots in polar coordinates as $r^{-2} = (\tilde{\eta}^2 + \tilde{\beta}^2)^{-1}$, $re^{\pm\beta} = \tilde{\eta} \pm \mathrm{i}\tilde{\beta}$. Let us first show the following lemma:

**Lemma 1.** *A matrix $M \in SL(3, \mathbb{Z})$ with complex eigenvalues as defined above has $\beta = 2\pi\frac{m}{n}$ if and only if it has at least one eigenvalue equal to 1.*

The proof of Lemma 1 requires the use of the following results. Let us consider $\varphi$, the Euler totient function where $\varphi(n)$ is the number of positive integers that are relatively prime to $n$. A scalar $\alpha$ is said to be algebraic over a field $K$ if there exists elements $a_0, \ldots, a_i, (i \geq 1)$ of $K$, not equal to zero, such that

$$\alpha_0 + \alpha a_1 + \cdots + \alpha^i a_i = 0,$$

and $\deg\{\alpha\}$ is the degree of the irreducible characteristic polynomial. We refer the reader to [30, Chapter 4] or any introduction to Algebra book for the background about the definitions used in this section. Then we have:

**Theorem 2.** *[46, Theorem 3.11] For $n > 4$ and $\gcd(m, n) = 1$,*

$$\deg\left\{\tan\frac{2m\pi}{n}\right\} = \begin{cases} \varphi(n) & \text{for } \gcd(n,8) < 4, \\ \frac{\varphi(n)}{2} & \text{for } \gcd(n,8) = 4, \\ \frac{\varphi(n)}{4} & \text{for } \gcd(n,8) > 4. \end{cases}$$

**Theorem 3.** *[2, Theorem 16.8.5] For $K$ the splitting field of an irreducible cubic polynomial $P$ over a field $\mathbb{Q}$ and $D_P$ the discriminant of $P$,*

- *If $D_P$ is a square in $\mathbb{Q}$, the degree of the extension field $K$ over $\mathbb{Q}$ is three*
- *If $D_P$ is not a square in $\mathbb{Q}$, the degree of the extension field $K$ over $\mathbb{Q}$ is six.*

We determine the degree of the algebraic integer $\tan\beta$ in the following lemma:

**Lemma 4.** $\tan\beta = \frac{\tilde{\beta}}{\tilde{\eta}}$ *is an algebraic integer of degree at most six.*

*Proof.* Since $\tilde{\eta}$ and $\tilde{\beta}$ are elements of the splitting field $K = \mathbb{Q}(r, e^{\beta})$ of the irreducible polynomial $P$, we have that $\frac{\tilde{\beta}}{\tilde{\eta}}$ is also an element of $K$. By Theorem 3, $K$ has a degree as most six in $\mathbb{Q}$ and so does $\frac{\tilde{\beta}}{\tilde{\eta}}$. □

Let us prove Lemma 1 by finding all coefficients $k, h \in \mathbb{Z}^+$ of the characteristic polynomial of $M$ for which $\beta = \frac{2m\pi}{n}, m, n \in \mathbb{Z}$.

| $\deg\left\{\tan\frac{2m\pi}{n}\right\}$ | $n$ |
|---|---|
| 1 | 1, 2 |
| 2 | 3, 6, 12, 16, 24 |
| 4 | 5, 10, 20, 32, 40, 48 |
| 6 | 7, 9, 14, 18, 28, 36, 56, 72 |

**Table 1.1:** Table of $n$ and $\deg\left\{\tan\frac{2m\pi}{n}\right\} \leq 6$

*Proof.* Let us assume that $\beta = \frac{2m\pi}{n}, m, n \in \mathbb{Z}$, and find the possible $n, m$ by using Theorem 2 and the Theorem 3 which guarantee that $\tan\frac{2m\pi}{n}$ is an algebraic integer of degree at most six. Thus using [39], we find all $n$ that satisfy the following

$$\begin{aligned}
\varphi(n) &\leq 6 \text{ for } \gcd(n,8) < 4,\\
\frac{\varphi(n)}{2} &\leq 6 \text{ for } \gcd(n,8) = 4,\\
\frac{\varphi(n)}{4} &\leq 6 \text{ for } \gcd(n,8) > 4,
\end{aligned}$$

and report all $n$ and $\deg\left\{\tan\frac{2m\pi}{n}\right\} \leq 6$ in Table 1.1. Then after some computation we find that

$$h = \frac{1 + 2r^3\cos 2\pi\frac{m}{n}}{r^2}, k = \frac{r^3 + 2\cos 2\pi\frac{m}{n}}{r},$$

and plugging in $n$ from the Table 1.1 and $m$ such that $\gcd(m,n) = 1$, we remark that $k, h \in \mathbb{Z}^+$ if $n = 1, 2$. In result, $P$ has at least one eigenvalue equal to 1, since $P(\lambda) = \lambda^3 - \lambda^2 + \lambda - 1$, or $P(\lambda) = \lambda^3 - 3\lambda^2 + 3\lambda - 1$ for the latter values of $n$. □

In sum, we derive the main corollary of this section:

**Corollary 1.** *The rotating box algorithm cannot give a time-periodic simulation box for any choice of integer commutative complex conjugate matrix.*

*Proof.* Using Lemma 1, we know that only matrices with an eigenvalue equal to one 1 have a rotational part that is a root of unity. However, those matrices are themselves pure rotations and have no use for the PBCs since they cannot control the stretching caused by the underlying background flow. □

## 1.6 Comparison of the three dimensional algorithms

In this section, we compute the minimum distance of the particle images for our algorithm and compare it with the GenKR algorithm.

To compute the minimum distance between a particle and its images when the rotating box PBCs is applied, we propose the matrix

$$M = \begin{bmatrix} 0 & -2 & 1 \\ 1 & 1 & 0 \\ 0 & 1 & 0 \end{bmatrix},$$

which has a pair of complex conjugate eigenvalues with positive real part. Then, the initial lattice is given by

$$L_0 = \begin{bmatrix} 0.9802 & 0.0658 & 0.2028 \\ 0.1109 & 1.3051 & -0.7165 \\ 0.4285 & 0.2442 & 0.7520 \end{bmatrix},$$

which implies that, given the standard lattice with the coordinate $(x, y, z)$, the $xy$ plane is rotated counterclockwise by approximately 113 degrees, and $xz$ by 111 degrees.

Moreover in the GenKR algorithm, we keep the automorphism matrices and the initial lattice given in the original paper but slightly modified the algorithms. As introduced in the earlier section, the GenKR algorithm presented in Algorithm 2, consists of applying an extra step of lattice basis reduction using the $LLL$ reduction algorithm on the remapped lattice obtained from Dobson's approach. We recall that GenKR uses the commutative matrices $M_i \in SL(3, \mathbb{Z})$ associated with the initial orthonormal lattice basis $L_0$, represented respectively as

$$M_1 = \begin{bmatrix} 1 & 1 & 1 \\ 1 & 2 & 2 \\ 1 & 2 & 3 \end{bmatrix}, M_2 = \begin{bmatrix} 2 & -2 & 1 \\ -2 & 3 & -1 \\ 1 & -1 & 1 \end{bmatrix} \text{and, } L_0 = \begin{bmatrix} 0.59101 & -0.73698 & 0.32799 \\ 0.73698 & 0.32799 & -0.59101 \\ 0.32799 & 0.59101 & 0.73698 \end{bmatrix}.$$

Then in Hunt's case, we find a matrix which has positive eigenvalues and which is commutative with the matrix given in the original paper. The commutative matrices $M_1, M_2$ and the normalized initial lattice $L_0$ respectively read

$$M_1 = \begin{bmatrix} 0 & 0 & 1 \\ 1 & 0 & -5 \\ 0 & 1 & 6 \end{bmatrix}, M_2 = \begin{bmatrix} 3 & 1 & 1 \\ -5 & -2 & -4 \\ 1 & 1 & 4 \end{bmatrix} \text{and, } L_0 = \begin{bmatrix} -2.1332 & -0.6570 & -0.2023 \\ -1.9624 & -1.2620 & -0.8116 \\ 0.0341 & 0.1723 & 0.8699 \end{bmatrix}.$$

**Algorithm 2** GenKR

$\Lambda_i = L_0 M_i L_0^{-1}$ ▷ Diagonalization of $M_i$
$\hat{\omega}_i = \text{diag}(\log(\Lambda_i))$ ▷ Compute the diagonal of the logarithm of $\Lambda_i$
$A = \delta_1 \hat{\omega}_1 + \delta_2 \hat{\omega}_2$ ▷ Compute $\delta_i$

$\theta_i = 0$ ▷ Initialize $\theta_i$
**for** $i = 1 \ldots$ Nsteps **do**
  $\theta_i \leftarrow \theta_i + \delta_k \tau t_*$ ▷ Update the time
  $\theta_i \leftarrow \theta_i - \lfloor \theta_i \rceil$ ▷ Find the decimal part of $\theta_i$
  $A_i \leftarrow \theta_1 \hat{\omega}_1 + \theta_2 \hat{\omega}_2$ ▷ Compute the remain stretch vector
  $\tilde{L}_i \leftarrow e^{\text{diag}(A_i)} L_0$ ▷ Compute the lattice value at the $i$ iteration
  $\hat{L}_i \leftarrow LLL(\tilde{L}_i)$ ▷ Reduce the remapped lattice with the $LLL$ reduction algorithm

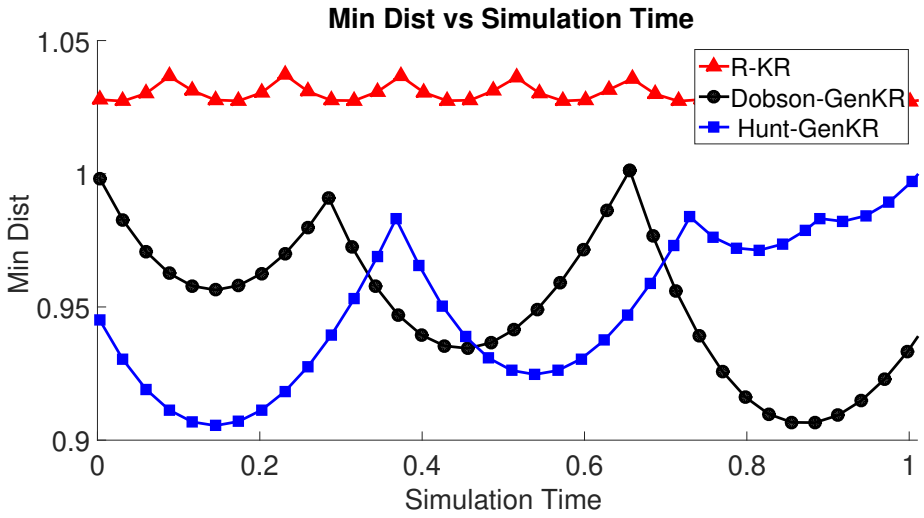


**Figure 1.5:** Minimum distance vs simulation time for our new algorithm (red triangle), GenKR (black circle) and, Hunt-GenKR (blue square). The minimum distance for the new algorithm is time-periodic, and is larger than the other PBCs' cases.

Then we graph the minimum distance for the three dimensional algorithms in figure 1.5, when the stretch is $\epsilon = 1$. We can observe in the graph that the minimum distance curve in rotating box PBCs case presents a clear pattern of periodicity. In

addition, the minimum distance over the simulation time interval for the rotating box algorithm is approximately 1.0271 compared to 0.9054 in GenKR's case.

## 1.7 Conclusion

Kraynik-Reinelt proved that it is impossible to find time periodic PBCs for general three dimensional flow, using $SL(3,\mathbb{Z})$ matrices with real eigenvalues. In this paper, we show that by using a $SL(3,\mathbb{Z})$ matrix with complex eigenvalues, we can create an algorithm that is time-periodic up to a rotation matrix for USF and BSF. Although we show that the rotations never align, the regularity of the remapping make this algorithm more straightforward than the existing ones. These PBCs also offer a better minimum distance between a particle and its images than the related GenKR scheme.

# CHAPTER 2

# CONVERGENCE OF NONEQUILIBRIUM LANGEVIN DYNAMICS FOR PLANAR FLOWS

**Note.** This chapter is accepted for publication to the Journal of Statistical Physics with the title: *"Convergence of Nonequilibrium Langevin Dynamics for Planar Flows", by Matthew Dobson and Abdel Kader A. Geraldo*

## 2.1 Abstract

We prove that incompressible two dimensional nonequilibrium Langevin dynamics (NELD) converges exponentially fast to a steady-state limit cycle. We use automorphism remapping periodic boundary conditions (PBCs) techniques such as Lees-Edwards PBCs and Kraynik-Reinelt PBCs to treat respectively shear flow and planar elongational flow. The convergence is shown using a technique similar to [ R. Joubaud, G. A. Pavliotis, and G. Stoltz,2014].

## 2.2 Introduction

A wide range of nonequilibrium molecular dynamics (NEMD) techniques [17, 62] are used in the study of molecular fluids under steady flow, and some recent applications can be found in [29, 48, 47, 44, 49, 45, 57, 40, 18, 36, 9, 64, 3, 59, 60]. Here

we study the exponential convergence of the probability density of nonequilibrium Langevin dynamics under incompressible two dimensional flows such as shear flow and planar elongational flow with spatial periodic boundary conditions (PBCs). We consider a molecular system corresponding to the micro-scale motion of a fluid with local strain rate $\nabla \mathbf{u}$ and denote the constant steady background flow matrix of the molecular system by $A = \nabla \mathbf{u} \in \mathbb{R}^{3\times 3}$. The coordinates of the simulation box are given by three linearly independent column vectors coming from the origin, and we write them in a matrix

$$L_t = \begin{bmatrix} \mathbf{v}_t^1 & \mathbf{v}_t^2 & \mathbf{v}_t^3 \end{bmatrix} \in \mathbb{R}^{3\times 3}, \qquad t \geq 0.$$

The initial simulation box is given by $L_0$ and the lattice deforms with the background flow according to the equation

$$L_t = e^{tA} L_0.$$

If $L_0$ is not chosen appropriately, the simulation box can become extremely stretched with degenerate geometry. For example, in the elongational flow case, if the compression is parallel to one of the edges of the simulation box, then the box will become degenerate to the point where a particle and its image become arbitrarily close. Thus, to perform a long simulation, we consider specialized PBCs consisting of a lattice automorphism represented as a $3 \times 3$ integer matrix with a determinant one to remap the simulation box at various times during the simulation. These types of PBCs were first used in the shear flow case by Lees and Edwards (LE) [31] and were then later

extended to the planar elongational flow case by Kraynik and Reinelt (KR) [28]. The analog of these types of PBCs that treats three dimensional flows such as uniaxial flow, biaxial flow, and generalized three-dimensional diagonalizable flow can be found in [13, 10, 24].

The NELD equation is written in terms of the relative momentum as

$$\begin{cases} d\widehat{\mathbf{q}} &= (\widehat{\mathbf{p}} + A\widehat{\mathbf{q}})dt, \\ d\widehat{\mathbf{p}} &= -\nabla V(\widehat{\mathbf{q}})dt - \gamma\widehat{\mathbf{p}}dt + \sigma dW, \end{cases} \tag{2.1}$$

where $V$ is the potential and $\sigma^2 = \frac{2\gamma}{\beta}$ is the fluctuation coefficient with $\beta$ being the inverse temperature. The position and the momentum of the particles are denoted by $(\widehat{\mathbf{q}}, \widehat{\mathbf{p}}) \in \widehat{\mathcal{L}}_t^d \times \mathbb{R}^{3d}$. Under the planar PBCs, the simulation box is represented by

$$\widehat{\mathcal{L}}_t = \{\widehat{L}_t\mathbf{x} \;\big|\; \mathbf{x} \in \mathbb{T}^3\}, \text{ where } \mathbb{T}^3 = \mathbb{R}^3 \backslash \mathbb{Z}^3, \tag{2.2}$$

$$\widehat{L}_t = e^{[t]A}L_0, \qquad \text{where } [t] \equiv t \bmod T, \tag{2.3}$$

where $\widehat{L}_t$ defines a remapped periodic lattice with a period of $T$. Although these remappings introduce a discontinuity in the simulation, the system as a whole remains homogeneous in space just as in [52, 9]. This is due to the fact that during the remapping, a particle within the simulation box is replaced by its image whose coordinates are denoted by $(\widehat{\mathbf{q}} + \widehat{L}\mathbf{n}, \widehat{\mathbf{p}})$ whose position satisfies (2.1):

$$d(\widehat{\mathbf{q}} + L_t\mathbf{n}) = (\widehat{\mathbf{p}} + A\widehat{\mathbf{q}} + AL_t\mathbf{n})dt \implies d\widehat{\mathbf{q}} = (\widehat{\mathbf{p}} + A\widehat{\mathbf{q}})dt,$$

as

$$\frac{d}{dt}L_t = AL_t.$$

Throughout this paper, we assume that the potential is smooth $V \in C^\infty$, which results in a finite gradient $\|\nabla V(\widehat{\mathbf{q}})\|_2 < \infty$ because the position space is compact. An example of an observable computed using the NELD is the bulk pressure tensor in a Lennard-Jones liquid [62]

$$\mathbf{f}(t, \widehat{\mathbf{q}}, \widehat{\mathbf{p}}) = \frac{1}{|\det \widehat{\mathcal{L}}_t|} \sum_{i=1}^{d} \Big( \|\widehat{\mathbf{p}}_i\|_2^2 - \frac{1}{2} \sum_{j \neq i}^{d} \mathbf{r}_{ij} \cdot \frac{\partial V}{\partial \mathbf{r}_{ij}}(\mathbf{r}_{ij}) \Big), \tag{2.4}$$

where $\mathbf{r}_{ij} = \|\widehat{\mathbf{q}}_i - \widehat{\mathbf{q}}_j\|_2$.

In the absence of a background flow, the domain of the simulation is stationary, and (2.1) becomes equilibrium Langevin Dynamics. It has been shown (see for instance [56, 37, 7, 33, 34, 4]) that under suitable conditions, the equilibrium Langevin Dynamics is ergodic with respect to the Boltzmann-Gibbs distribution

$$\nu(\widehat{\mathbf{q}}, \widehat{\mathbf{p}}) d\widehat{\mathbf{q}} d\widehat{\mathbf{p}} = \frac{1}{Z} e^{-\beta H(\widehat{\mathbf{q}}, \widehat{\mathbf{p}})} d\widehat{\mathbf{q}} d\widehat{\mathbf{p}}, \quad Z = \int_{\mathcal{L}_0^d \times \mathbb{R}^{3d}} e^{-\beta H(\widehat{\mathbf{q}}, \widehat{\mathbf{p}})} d\widehat{\mathbf{q}} d\widehat{\mathbf{p}},$$

where $Z$ is the normalization constant, and $H$ is the Hamiltonian of the system given by

$$H(\widehat{\mathbf{q}}, \widehat{\mathbf{p}}) = \frac{1}{2} \langle \widehat{\mathbf{p}}, \widehat{\mathbf{p}} \rangle + V(\widehat{\mathbf{q}}).$$

However, convergence to a limiting measure has not been established for NELD under moving domains.

In this paper, we show the existence, uniqueness, and exponential convergence of the planar flow case of NELD to a time-periodic invariant measure referred to as a limit cycle, following the work done in [26]. To accomplish this, it will be necessary to reformulate the NELD within a fixed domain in order to show the regularity of the probability distribution. In addition, we will construct a Markov chain at integer multiples of the remapping time, established when the particles are in the initial box $\mathcal{L}_0$. This Markov chain can be utilized to show both the existence and uniqueness of an invariant measure at the remapping times. In Section 2.3, we present the derivation of the particle remapping function. The main result of the paper is then established in Section 2.4, where we prove the convergence of the NELD to a probability density function, as shown in Proposition 1.

## 2.3 Time-Periodic Remapping

First, we derive the remapping of the simulation box under LE and KR PBCs. Next, we proceed to define the remapping function of the particle coordinates while the simulation box is being remapped.

### 2.3.1 Remapping the Unit Cell

We start by defining the remapped Eulerian domain in the shear flow case, followed by the planar elongational flow case.

#### 2.3.1.1 Shear Case

We denote the background matrix of the shear flow by

$$A = \begin{bmatrix} 0 & \epsilon & 0 \\ 0 & 0 & 0 \\ 0 & 0 & 0 \end{bmatrix}, \ \epsilon \in \mathbb{R}^*.$$

At a time $t$, the basis vectors for the simulation box are the columns of the matrix

$$L_t = \begin{bmatrix} 1 & t\epsilon & 0 \\ 0 & 1 & 0 \\ 0 & 0 & 1 \end{bmatrix} L_0 \text{ where } L_0 = \begin{bmatrix} 1 & 0 & 0 \\ 0 & 1 & 0 \\ 0 & 0 & 1 \end{bmatrix}.$$

Since $L_t$ is highly sheared as $t$ becomes large, the interparticle interaction computation becomes more difficult. We can prevent this anomaly by applying the LE PBCs which consists in multiplying $L_t$ by the lattice automorphism matrix

$$M^k = \begin{bmatrix} 1 & -1 & 0 \\ 0 & 1 & 0 \\ 0 & 0 & 1 \end{bmatrix}^k = \begin{bmatrix} 1 & -k & 0 \\ 0 & 1 & 0 \\ 0 & 0 & 1 \end{bmatrix}, \quad k \in \mathbb{Z},$$

to get the remapped simulation box lattice

$$L_t M^k = \begin{bmatrix} 1 & t\epsilon - k & 0 \\ 0 & 1 & 0 \\ 0 & 0 & 1 \end{bmatrix}, k \in \mathbb{Z}.$$

Since $M$ is an integer matrix with determinant equal to one ($M \in SL(3,\mathbb{Z})$), the lattice basis vectors in $L_t$ and $L_t M^k$ generate the same lattice. By choosing $k = -\lfloor t\epsilon \rceil$, where $\lfloor x \rceil$ denotes $x$ rounded to the nearest integer, we ensure that the stretch is at most half of the simulation box. Then we observe that the stretch matrix is time-periodic with the period $T = \frac{1}{\epsilon}$, and discontinuous at time multiple of $T$:

$$\begin{bmatrix} 0 & t\epsilon - \lfloor t\epsilon \rceil & 0 \\ 0 & 0 & 0 \\ 0 & 0 & 0 \end{bmatrix} = [t]\epsilon D, \quad \text{where } D = \begin{bmatrix} 0 & 1 & 0 \\ 0 & 0 & 0 \\ 0 & 0 & 0 \end{bmatrix}, \ [t] = \theta \equiv t \bmod T. \tag{2.5}$$

This implies that the particle position belongs to remapped Eulerian domain

$$\widehat{\mathcal{L}}_t = \{e^{[t]A} L_0 \mathbf{x} \big| \mathbf{x} \in \mathbb{T}^3\}, \text{ where } \mathbb{T}^3 = \mathbb{R}^3 \backslash \mathbb{Z}^3. \tag{2.6}$$

In the Section 2.3.2, we analyse the particles remapped position in $\widehat{\mathcal{L}}_t$ and in the unit cell.

#### 2.3.1.2 Planar Elongational Flow Case

We consider the planar elongational flow (PEF) case with background flow matrix given by

$$A = \begin{bmatrix} \epsilon & 0 & 0 \\ 0 & -\epsilon & 0 \\ 0 & 0 & 0 \end{bmatrix}, \ \epsilon \in \mathbb{R}^*,$$

which means that the simulation box elongates in the $x$ direction and shrinks in the $y$ direction of the standard coordinate plane. As $t$ goes to infinity, a particle and its image can become arbitrarily close if an edge of the simulation box is aligned with the $y$ coordinate. This would lead to a breakdown in the simulation. We prevent this issue by applying the KR PBCs, which consists in carefully choosing the alignment of the initial simulation box and remapping the simulation box with a matrix $M \in SL(3, \mathbb{Z})$. We choose $M$ such that it is diagonalizable with eigenvalues of the form

$$MS = S\Lambda, \quad \Lambda = \begin{bmatrix} \lambda & 0 & 0 \\ 0 & \lambda^{-1} & 0 \\ 0 & 0 & 1 \end{bmatrix}, \quad \lambda > 0, \quad \lambda \neq 1.$$

We choose the initial lattice $L_0 = S^{-1}$ rather than the standard coordinate directions, and this will prevent particle images from becoming too close. If we remap the lattice basis vectors by applying $M^k$, we get

$$L_t M^k = e^{tA} L_0 M^k = e^{t\epsilon D} \Lambda^n S^{-1} = e^{(t\epsilon + k\eta)D} S^{-1},$$
$$\text{where } D = \begin{bmatrix} 1 & 0 & 0 \\ 0 & -1 & 0 \\ 0 & 0 & 0 \end{bmatrix}, \quad \eta = \log(\lambda).$$

Letting $T = \frac{\eta}{\epsilon}$, the stretched matrix $[t]A$ and the position domain of the particles are also respectively expressed in the periodic form as in (2.5) and (2.6).

### 2.3.2 Remapping of the Particle Coordinates

We will formulate the dynamics with remappings of the particle positions. While this does lead to discontinuities of the particle paths in real space, it is not a true discontinuity of the system. When the particles are remapped, we are choosing a different image particle to track, but the set of all periodic images of the tracked particle is unchanged when considered in $\mathbb{R}^3$. This is the same effect of applying spatial periodic boundary conditions whenever a particle in the simulation would move outside the simulation box.

Now, we define the function which remaps the particle positions when the unit cell is remapped at multiples of the period $kT$. This function chooses the image particle that lives within the unit cell for the remapped lattice. We start by defining the modulus operation applied to each vector component

$$\mathbf{g}(\mathbf{x}) \equiv \mathbf{x} \bmod 1, \text{ where } \mathbf{x} \in \mathbb{R}^3.$$

At time $T$, we denote the simulation box before remapping by $\mathcal{L}_{T^-}$ and after remapping by $\mathcal{L}_T$, where we note that by definition, $\mathcal{L}_T = \mathcal{L}_0$. Let us define by $\overline{\mathbf{g}} : \widehat{\mathcal{L}}_{T^-} \to \widehat{\mathcal{L}}_0$:

$$\widehat{\mathbf{q}}_{kT} = \overline{\mathbf{g}}(\widehat{\mathbf{q}}_{kT^-}) = L_0\, \mathbf{g}\left(L_0^{-1}\widehat{\mathbf{q}}_{kT^-}\right), \tag{2.7}$$

which maps the particle positions after the simulation box is remapped. Since the momentum is not affected by the remapping, the function

$$\mathfrak{R}_T : \widehat{\mathcal{L}}^d_{T^-} \times \mathbb{R}^{3d} \to \widehat{\mathcal{L}}^d_0 \times \mathbb{R}^{3d} \quad (\widehat{\mathbf{q}}_{kT}, \widehat{\mathbf{p}}_{kT}) = (\overline{\mathbf{g}}(\widehat{\mathbf{q}}_{kT^-}), \widehat{\mathbf{p}}_{kT^-}),$$

describes the remapping of particle coordinates.

## 2.4 Ergodicity of NELD under Planar Flow

We start this section by deriving the forward and backward Kolmogorov equation of the NELD and show the regularity property of the NELD in Section 2.4.1, then build on the latter result to prove the main result of the paper, the convergence of the NELD to a measure in Section 2.4.4.

### 2.4.1 Markov Process Generator

We derive the generator of the NELD and use it to find the forward and backward Kolmogorov equations. Then, we establish the regularity of the NELD by showing that its transition kernel is smooth and positive using respectively[8, Lemma A.5] and [4, Corollary 6.2].

#### 2.4.1.1 Fokker-Planck Equation

The NELD dynamics (2.1) can be written in vector form as

$$\begin{cases} d\widehat{\mathbf{X}}_t = \widehat{\mathbf{b}}(\widehat{\mathbf{X}}_t)dt + \widehat{\Sigma}dW_t, \quad \widehat{\mathbf{X}}_t \in \widehat{\mathcal{L}}_t^d \times \mathbb{R}^{3d}, \qquad t \in [kT, (k+1)T), \\ \widehat{\mathbf{X}}_t = \begin{bmatrix} \widehat{\mathbf{q}} \\ \widehat{\mathbf{p}} \end{bmatrix}, \quad \widehat{\mathbf{b}}(\widehat{\mathbf{X}}_t) = \begin{bmatrix} \widehat{\mathbf{p}} + A\widehat{\mathbf{q}} \\ -\nabla V(\widehat{\mathbf{q}}) - \gamma\widehat{\mathbf{p}} \end{bmatrix}, \quad \widehat{\Sigma} = \begin{bmatrix} 0 & 0 \\ 0 & \sigma \end{bmatrix}, \end{cases} \tag{2.8}$$

with $\widehat{\mathbf{X}}_{kT} = \mathfrak{R}(\widehat{\mathbf{X}}_{kT^-})$ at the remapping time $t_k = kT$. Applying Itô's lemma to any smooth function $\widehat{\mathbf{f}}_t \in C^\infty(\mathbb{R} \times \widehat{\mathcal{L}}_t^d \times \mathbb{R}^{3d}; \mathbb{R})$, yields

$$d\widehat{\mathbf{f}}_t(\widehat{\mathbf{X}}_t) = \big(\partial_t \widehat{\mathbf{f}}_t + G\widehat{\mathbf{f}}_t\big)(\widehat{\mathbf{X}}_t)dt + \Big\langle \nabla \widehat{\mathbf{f}}_t(\widehat{\mathbf{X}}_t), \widehat{\Sigma} dW \Big\rangle,$$

where

$$G = \langle \widehat{\mathbf{p}} + A\widehat{\mathbf{q}}, \nabla_{\widehat{\mathbf{q}}} \cdot \rangle + \langle -\nabla V(\widehat{\mathbf{q}}), \nabla_{\widehat{\mathbf{p}}} \cdot \rangle - \gamma \langle \widehat{\mathbf{p}}, \nabla_{\widehat{\mathbf{p}}} \cdot \rangle + \frac{1}{2}\sigma\sigma^T : \nabla^2,$$

is the infinitesimal generator. The symbols : and $\langle \cdot, \cdot \rangle$ denote the Frobenius inner product. Now let us write the strong solution of (2.8) as

$$\widehat{\mathbf{X}}_t - \widehat{\mathbf{X}}_s = \int_s^t \mathbf{b}(\widehat{\mathbf{X}}_u)du + \widehat{\Sigma} dW_u, \quad s \le u < t, \ s, t \in [kT, (k+1)T),$$

and at the remapping time $t_k$, we have $\widehat{\mathbf{X}}_{kT} = \mathfrak{R}(\widehat{\mathbf{X}}_{kT^-})$. The density transition function from one state to another in the is defined by

$$\widehat{\mathcal{P}}_{t,s}(\widehat{\mathbf{y}}, \widehat{B}_t) = \mathbb{P}\big(\widehat{\mathbf{X}}_t \in \widehat{B}_t \big| \widehat{\mathbf{X}}_s = \widehat{\mathbf{y}}\big) = \int_{\widehat{B}_t} \widehat{\psi}(t, \widehat{\mathbf{x}} \big| s, \widehat{\mathbf{y}}) d\widehat{\mathbf{x}},$$
$$\text{where } \ \widehat{\psi}(t, \widehat{\mathbf{x}} \,|s, \widehat{\mathbf{y}})\Big|_{t=s} = \delta(\widehat{\mathbf{x}} - \widehat{\mathbf{y}}),$$

$\forall \widehat{\mathbf{x}} \in \widehat{\mathcal{L}}_t^d \times \mathbb{R}^{3d}$, $\widehat{B}_t \in \mathcal{B}(\widehat{\mathcal{L}}_t^d \times \mathbb{R}^{3d})$, and the generator is found by taking the expectation of a smooth function $\widehat{\mathbf{f}}_t \in C^\infty(\mathbb{R} \times \widehat{\mathcal{L}}_t^d \times \mathbb{R}^{3d}; \mathbb{R})$ with respect to the probability density function $\widehat{\psi}$:

$$\widehat{\phi}_{t,s}(\widehat{\mathbf{y}}) = \mathbb{E}^{s,\mathbf{y}}[\widehat{\mathbf{f}}_t(\widehat{\mathbf{X}}_t)] = \int_{\widehat{\mathcal{L}}_t^d \times \mathbb{R}^{3d}} \widehat{\mathbf{f}}_t(\widehat{\mathbf{x}}) \widehat{\psi}(t, \widehat{\mathbf{x}} \big| s, \widehat{\mathbf{y}}) d\widehat{\mathbf{x}}, \tag{2.9}$$
$$s \le t, \ s, t \in [kT, (k+1)T).$$

Now we derive the backward Kolmogorov equation for the NELD in the following lemma:

**Lemma 5.** *[19, Theorem 6.1] The backward Kolmogorov equation for the NELD is*

$$\partial_s \widehat{\phi}_{t,s}(\widehat{\mathbf{y}}) + \big(G\widehat{\phi}_{t,s}\big)(\widehat{\mathbf{y}}) = 0, \quad \textit{where} \quad \widehat{\psi}(t,\widehat{\mathbf{x}}\,|s,\widehat{\mathbf{y}})\Big|_{t=s} = \delta(\widehat{\mathbf{x}}-\widehat{\mathbf{y}}), \tag{2.10}$$

The forward Kolmogorov equation of the NELD is given in the following lemma:

**Lemma 6.** *The forward Kolmogorov equation of the NELD is*

$$\big(-\partial_t\widehat{\psi} + G^{\dagger}\widehat{\psi}\big)(t,\widehat{\mathbf{x}}\big|s,\widehat{\mathbf{y}}) = 0. \tag{2.11}$$

The proof of this Lemma is obtained by using the adjoint property to have

$$\begin{aligned}\int_{\widehat{\mathcal{L}}_t^d\times\mathbb{R}^{3d}} \big(\partial_t\widehat{\mathbf{f}}_t + G\widehat{\mathbf{f}}_t\big)(\widehat{\mathbf{x}})\widehat{\psi}(t,\widehat{\mathbf{x}}\big|s,\widehat{\mathbf{y}})d\widehat{\mathbf{x}} \\ = \int_{\widehat{\mathcal{L}}_t^d\times\mathbb{R}^{3d}} \widehat{\mathbf{f}}_t(\widehat{\mathbf{x}})\big(-\partial_t\widehat{\psi} + G^{\dagger}\widehat{\psi}\big)(t,\widehat{\mathbf{x}}\big|s,\widehat{\mathbf{y}})d\widehat{\mathbf{x}}.\end{aligned}$$

and by applying (2.11). Note that the probability density of $\widehat{\mathbf{X}}_t$, denoted by

$$\nu(t,\widehat{\mathbf{x}}) = \int_{\widehat{\mathcal{L}}_t^d\times\mathbb{R}^{3d}} \widehat{\psi}(t,\widehat{\mathbf{x}}\big|s,\overline{\mathbf{y}})\nu(s,\overline{\mathbf{y}})d\overline{\mathbf{y}}$$

satisfies the forward Kolmogorov equation, and the backward evolution from $\widehat{\phi}_{t',t}(t,\widehat{\mathbf{x}})$ to $\widehat{\phi}_{t,s}(s,\widehat{\mathbf{y}}),\ s\le t\le t'$ satisfies

$$\widehat{\phi}_{t,s}(s,\widehat{\mathbf{y}}) = \int_{\widehat{\mathcal{L}}_t^d\times\mathbb{R}^{3d}} \widehat{\phi}_{t',t}(t,\widehat{\mathbf{x}})\widehat{\psi}(t,\widehat{\mathbf{x}}\big|s,\widehat{\mathbf{y}})d\widehat{\mathbf{x}}.$$

### 2.4.2 Markov Process Generator in a Fixed Domain

We derive the NELD equation and its Markov process generator in a fixed domain to show the transition kernel's regularity in the moving domain in the next section.

#### 2.4.2.1 NELD with LE and KR PBCs in Fixed Coordinates

We write the NELD equation in a fixed domain by considering the change of variables

$$\begin{cases} \widehat{\mathbf{q}}_t = e^{[t]A}\overline{\mathbf{q}}_t \\ \widehat{\mathbf{p}}_t = e^{[t]A}\overline{\mathbf{p}}_t \end{cases}, \ (\overline{\mathbf{q}},\overline{\mathbf{p}}) \in \mathcal{L}_0^d \times \mathbb{R}^{3d}, \ (\widehat{\mathbf{q}},\widehat{\mathbf{p}}) \in \widehat{\mathcal{L}}_t^d \times \mathbb{R}^{3d}. \tag{2.12}$$

Next, we compute the time derivative of the position when $\frac{t}{T} \notin \mathbb{Z}$ to have:

$$d\widehat{\mathbf{q}}_t = e^{[t]A}\Big(d\overline{\mathbf{q}} + A\overline{\mathbf{q}}dt\Big) = (\widehat{\mathbf{p}} + A\widehat{\mathbf{q}})dt,$$

which implies that

$$d\overline{\mathbf{q}} = \overline{\mathbf{p}}dt.$$

Computing the time derivative of the momentum when $\frac{t}{T} \notin \mathbb{Z}$ gives

$$\begin{aligned} d\overline{\mathbf{p}} =& - Ae^{-[t]A}\Big(\widehat{\mathbf{p}} - A\widehat{\mathbf{p}}\Big)dt \\ =& - e^{-[t]A}\nabla V(e^{[t]A}\overline{\mathbf{q}})dt - (A+\gamma)\overline{\mathbf{p}}dt + \sigma e^{-[t]A}dW. \end{aligned}$$

This leads to the NELD equation written in the fixed domain:

$$\begin{cases} d\overline{\mathbf{q}}_t &= \overline{\mathbf{p}}_t dt, \\ d\overline{\mathbf{p}}_t &= -e^{-[t]A}\nabla V\big(e^{[t]A}\overline{\mathbf{q}}_t\big)dt - \Gamma\overline{\mathbf{p}}_t dt + \sigma e^{-[t]A}dW_t \end{cases}, \quad \frac{t}{T} \notin \mathbb{Z}, \tag{2.13}$$

where $\Gamma = A + \gamma$.

#### 2.4.2.2 Markov Process Generator

Let us rewrite (2.13) as,

$$\begin{cases} d\overline{\mathbf{X}}_t = \overline{\mathbf{b}}_t(\overline{\mathbf{X}}_t)dt + \overline{\Sigma}_t dW_t, \ \frac{t}{T} \notin \mathbb{Z}, \quad \overline{\mathbf{X}}_t \in \mathcal{L}_0^d \times \mathbb{R}^{3d} \\ \overline{\mathbf{X}}_t = \begin{bmatrix} \overline{\mathbf{q}} \\ \overline{\mathbf{p}} \end{bmatrix}, \quad \overline{\mathbf{b}}_t(\overline{\mathbf{X}}_t) = \begin{bmatrix} \overline{\mathbf{p}} \\ -e^{-[t]A}\nabla V(e^{[t]A}\overline{\mathbf{q}}) - \Gamma\overline{\mathbf{p}} \end{bmatrix}, \quad \overline{\Sigma}_t = \begin{bmatrix} 0 & 0 \\ 0 & \sigma e^{-[t]A} \end{bmatrix}, \end{cases} \tag{2.14}$$

and express the strong solution of the latter equation as

$$\overline{\mathbf{X}}_t - \overline{\mathbf{X}}_s = \int_s^t \overline{\mathbf{b}}_u(\overline{\mathbf{X}}_u)du + \overline{\Sigma}_u dW_u, \quad s \le u < t, \ s,t \in [kT,(k+1)T).$$

Then, we define the density transition function from one state to another in the continuous-time Markov chain $\overline{\mathbf{X}}_t$ by

$$\mathbb{P}\big(\overline{\mathbf{X}}_t \in \overline{B}\big|\overline{\mathbf{X}}_s = \overline{\mathbf{y}}\big) = \int_{\overline{B}} \overline{\psi}(t,\overline{\mathbf{x}}\big|s,\overline{\mathbf{y}})d\overline{\mathbf{x}}, \text{ where } \psi(t,\overline{\mathbf{x}}\,|t,\overline{\mathbf{y}}) = \delta(\overline{\mathbf{x}} - \overline{\mathbf{y}}),$$

$\forall \overline{\mathbf{x}} \in \mathcal{L}_0^d \times \mathbb{R}^{3d},\ \overline{B} \in \mathcal{B}(\mathcal{L}_0^d \times \mathbb{R}^{3d})$ . Using the change of variables (2.12), we define the mapping of the coordinates from the fixed domain to the moving domain by

$$\Phi_t : \mathcal{L}_0^d \times \mathbb{R}^{3d} \to \widehat{\mathcal{L}}_t^d \times \mathbb{R}^{3d} \quad \begin{bmatrix} \widehat{\mathbf{q}}_t \\ \widehat{\mathbf{p}}_t \end{bmatrix} = \begin{bmatrix} e^{[t]A} & 0 \\ 0 & e^{[t]A} \end{bmatrix} \begin{bmatrix} \overline{\mathbf{q}}_t \\ \overline{\mathbf{p}}_t \end{bmatrix}.$$

Thus the expectation $\widehat{\mathbf{f}}_t(\widehat{\mathbf{X}}) = (\mathbf{f}_t \circ \Phi_t)(\overline{\mathbf{X}}_t) \in C^\infty(\mathbb{R} \times \mathcal{L}_0^d \times \mathbb{R}^{3d}; \mathbb{R})$ with respect to the probability density function $\overline{\psi}$ is writing as

$$\overline{\phi}_{t,s}(\overline{\mathbf{y}}) = \mathbb{E}^{s,\mathbf{y}}(\mathbf{f}_t \circ \Phi_t)(\overline{\mathbf{X}}_t) = \int_{\mathcal{L}_0^d \times \mathbb{R}^{3d}} (\mathbf{f}_t \circ \Phi_t)(\overline{\mathbf{x}}) \overline{\psi}(t, \overline{\mathbf{x}} \big| s, \overline{\mathbf{y}}) d\overline{\mathbf{x}},$$
$$s \le t,\ s, t \in [kT, (k+1)T).$$

We write the generator of (2.13) as follows:

$$\overline{G} = \overline{\mathcal{X}}_0 + \frac{1}{2} \sum_{i=1}^{d} \overline{\mathcal{X}}_i,\ \text{for } 1 \le i \le d,$$

where

$$\overline{\mathcal{X}}_0 = \langle \overline{\mathbf{p}}, \nabla_{\overline{\mathbf{q}}} \cdot \rangle - \left\langle e^{-[t]A} \nabla V(e^{[t]A} \overline{\mathbf{q}}), \nabla_{\overline{\mathbf{p}}} \cdot \right\rangle - \langle \Gamma \overline{\mathbf{p}}, \nabla_{\overline{\mathbf{p}}} \cdot \rangle$$
$$\overline{\mathcal{X}}_i = \sqrt{\frac{2\gamma}{\beta}} s_{j,i} \partial_{\overline{\mathbf{p}}_i}, \quad (s_{j,i}) = e^{-[t]A} (e^{-[t]A})^T.$$

Similarly to the dynamics in the moving domain, we write the backward and forward Kolmogorov equations, now in the time inhomogeneous case:

**Lemma 7.** *[19, Theorem 6.1] The backward Kolmogorov equation for the NELD is*

$$\partial_s \overline{\phi}_{t,s}(\overline{\mathbf{y}}) + \big(\overline{G}_s \overline{\phi}_{t,s}\big)(\overline{\mathbf{y}}) = 0, \quad \textit{where} \quad \overline{\psi}(t, \overline{\mathbf{x}}\,|s, \overline{\mathbf{y}})\big|_{t=s} = \delta(\overline{\mathbf{x}} - \overline{\mathbf{y}}).$$

The forward Kolmogorov equation of the NELD is given in the following lemma:

**Lemma 8.** *The forward Kolmogorov equation of the NELD is*

$$\big( - \partial_t \overline{\psi} + \overline{G}_s^{\dagger} \overline{\psi}\big)(t, \overline{\mathbf{x}}\big|s, \overline{\mathbf{y}}) = 0. \tag{2.15}$$

The probability density of $\overline{\mathbf{X}}_t$ denoted by,

$$\overline{\nu}(t, \overline{\mathbf{x}}) = \int_{\mathcal{L}_0^d \times \mathbb{R}^{3d}} \overline{\psi}(t, \overline{\mathbf{x}}\big|s, \overline{\mathbf{y}}) \overline{\nu}(s, \overline{\mathbf{y}}) d\overline{\mathbf{y}}$$

satisfies the forward Kolmogorov equation and the backward evolution from $\overline{\phi}_{t',t}(t, \overline{\mathbf{x}})$ to $\overline{\phi}_{t,s}(s, \overline{\mathbf{y}}),\ s \leq t \leq t'$ satisfies

$$\overline{\phi}_{t,s}(s, \overline{\mathbf{y}}) = \int_{\mathcal{L}_0^d \times \mathbb{R}^{3d}} \overline{\phi}_{t',t}(t, \overline{\mathbf{x}}) \overline{\psi}(t, \overline{\mathbf{x}}\big|s, \overline{\mathbf{y}}) d\overline{\mathbf{x}}.$$

### 2.4.3 Regularity of the NELD

The smoothness of the transition kernel of $\overline{\mathbf{X}}$ on an interval $[kT, (k+1)T)$ is obtained by using the result from [8, Lemma A.5], and the positivity is obtained using a standard control theory argument.

#### 2.4.3.1 Smoothness

First, we show that $\overline{G}_t, \frac{[t]}{T} \notin \mathbb{Z}$ is hypoelliptic in the following Lemma:

**Lemma 9.** *$\partial_t + \overline{G}_t, -\partial_t + \overline{G}_t^\dagger, \frac{[t]}{T} \notin \mathbb{Z}$ are hypoelliptic.*

*Proof.* We define $\mathfrak{L}(\overline{\mathcal{X}}_0, \ldots, \overline{\mathcal{X}}_d)$, the Lie algebra of the family of the vectorial space operators $(\overline{\mathcal{X}}_0, \ldots, \overline{\mathcal{X}}_d) \in \text{Span}(\overline{\mathcal{X}}_0, \ldots, \overline{\mathcal{X}}_d)$ satisfying the stability property:

$$B \in \mathfrak{L}(\overline{\mathcal{X}}_0, \ldots, \overline{\mathcal{X}}_d) \implies [B, \overline{\mathcal{X}}_i] \in \mathfrak{L}(\overline{\mathcal{X}}_0, \ldots, \overline{\mathcal{X}}_d), \quad i = 0, \ldots, d,$$

where the Lie bracket between two operators $\mathscr{C}$ and $\mathscr{D}$ is

$$[\mathscr{C}, \mathscr{D}] = \mathscr{C}\mathscr{D} - \mathscr{D}\mathscr{C}.$$

Since for every point $(\overline{\mathbf{q}}_{kT+\theta}, \overline{\mathbf{p}}_{kT+\theta}) \in \mathcal{L}_0^d \times \mathbb{R}^{3d}$, we have

$$[\overline{\mathcal{X}}_i, \overline{\mathcal{X}}_0] = \sqrt{\frac{\gamma}{2\beta}}(\partial_{\overline{\mathbf{q}}_i} + \gamma s_{i,j})\partial_{\overline{\mathbf{p}}_i}, \quad \forall i \in \{1 \ldots d\},$$

evaluated at $(\overline{\mathbf{q}}_0, \overline{\mathbf{p}}_0)$ span $\mathcal{L}_0^d \times \mathbb{R}^{3d}$, it follows that $\overline{G}_t$ and $\overline{G}_t^\dagger$ are hypoelliptic using [23, Theorem 1.1]. □

**Lemma 10.** *[8, Lemma A.5] If $-\partial_t + \overline{G}_t^\dagger$ is hypoelliptic and there exists $\overline{\nu}_t(\cdot)$, $t \in [kT, (k+1)T]$ such that*

$$\big( - \partial_t \overline{\nu}_t + \overline{G}_t^\dagger \overline{\nu}_t \big)(\cdot) = 0,$$

*then $\overline{\nu}_t(\cdot) \in C^\infty, \frac{[t]}{T} \notin \mathbb{Z}$ .*

Now, we derive the smoothness of the Markov process generator of $\overline{\mathbf{X}}_t$ and $\widehat{\mathbf{X}}_t$ in the following Lemma:

**Lemma 11.** *The Markov process generator of* $\overline{\mathbf{X}}_t$ *and* $\widehat{\mathbf{X}}_t$ *are smooth and we have:*

$$\mathbb{E}^{s,\mathbf{y}}\mathbf{f}_t(\widehat{\mathbf{X}}_t) = \mathbb{E}^{s,\mathbf{y}}[(\mathbf{f}_t \circ \Phi_t)(\overline{\mathbf{X}}_t)], \quad \frac{t}{T} \notin \mathbb{Z}.$$

*Proof.* Using Lemma 10, we have the transition map $\overline{\psi}$ for $\overline{\mathbf{X}}_t$ is smooth. Next, we have

$$\begin{aligned}
\mathbb{E}^{s,\mathbf{y}}(\mathbf{f} \circ \Phi_t)(\overline{\mathbf{X}}_t) &= \int_{\mathcal{L}_0^d \times \mathbb{R}^{3d}} (\mathbf{f} \circ \Phi_t)(\overline{\mathbf{x}}) \overline{\psi}(t, \overline{\mathbf{x}} \big| s, \overline{\mathbf{y}}) d\overline{\mathbf{x}} \\
&= \int_{\widehat{\mathcal{L}}_t^d \times \mathbb{R}^{3d}} \mathbf{f}(\widehat{\mathbf{x}}) (\overline{\psi} \circ \Phi_t^{-1})(t, \widehat{\mathbf{x}} \big| s, \widehat{\mathbf{y}}) d\widehat{\mathbf{x}} \\
&= \int_{\widehat{\mathcal{L}}_t^d \times \mathbb{R}^{3d}} \mathbf{f}(\widehat{\mathbf{x}}) \widehat{\psi}(t, \widehat{\mathbf{x}} \big| s, \widehat{\mathbf{y}}) d\widehat{\mathbf{x}},
\end{aligned}$$

where $\widehat{\psi} = \overline{\psi} \circ \Phi_t^{-1}$. Therefore, $\widehat{\psi}(t, \widehat{\mathbf{x}} \big| \cdot)$ is smooth. □

#### 2.4.3.2 Positivity

Now, we will show that the bounded periodic domain $\widehat{B}_t \in \mathcal{B}(\widehat{\mathcal{L}}_t^d \times \mathbb{R}^{3d})$ can be reached at any time with a positive transition kernel $\widehat{\mathcal{P}}_{t,0}(\widehat{\mathbf{y}}, \widehat{B}_t) > 0$, using a method similar to the control theory technique developed in [4, Section 6] and [37]. Intuitively, the control approach replaces the noise term with a control, showing the accessible configurations of the stochastic system. We first establish that the control has a positive kernel, and then prove that it approximates the NELD.

**Lemma 12.** *$G_t$ has a positive transition kernel.*

*Proof.* Let us consider the following associated control problem, derived from (2.8):

$$\frac{d\widetilde{\mathbf{X}}_t}{dt} = \mathbf{b}(\widetilde{\mathbf{X}}_t) + \widehat{\Sigma}\frac{d\mathcal{U}_t}{dt}, \quad \widetilde{\mathbf{X}}_t = \begin{bmatrix} \widetilde{\mathbf{q}} \\ \widetilde{\mathbf{p}} \end{bmatrix} \in \widehat{\mathcal{L}}_t^d \times \mathbb{R}^{3d}, \tag{2.16}$$

with $\widetilde{\mathbf{X}}_{kT} = \mathfrak{R}(\widetilde{\mathbf{X}}_{kT^-})$ at the remapping time $t_k = kT$. For $t > 0$ and two points $(\widetilde{\mathbf{q}}_0, \widetilde{\mathbf{p}}_0)$ and $(\widetilde{\mathbf{q}}_t, \widetilde{\mathbf{p}}_t)$, we can find smooth $\mathcal{U}_t \in C^\infty([0,t], \mathbb{R}^{3d})$ such that (2.16) is satisfied. In addition, there is $\mathcal{C}^2$ path denoted by $\varphi(t)$ in $\mathbb{R}^{3d}$, defined from $\mathcal{L}_0^d \times \mathbb{R}^{3d}$ to $\widehat{\mathcal{L}}_t^d \times \mathbb{R}^{3d}$, and satisfies $\varphi(0) = \widetilde{\mathbf{q}}_0$, $\varphi(t) = \widetilde{\mathbf{q}}_t$, $\varphi^{'}(0) = \widetilde{\mathbf{p}}_0$, and $\varphi^{'}(t) = \widetilde{\mathbf{p}}_t + A\widetilde{\mathbf{q}}_t$. This can be shown by setting

$$\widetilde{\mathbf{X}}_t = \begin{bmatrix} \varphi(t) \\ \varphi^{'}(t) \end{bmatrix}, \quad \text{then } \mathcal{V}_t = \frac{d\mathcal{U}_t}{dt} = \sqrt{\frac{2\beta}{\gamma}}\Big(\ddot{\varphi}_t + \nabla V(\varphi_t) - A\varphi_t + \gamma\dot{\varphi}_t\Big),$$

where $\mathcal{V}_t$ is a smooth control. This because $\nabla V \in C^\infty$. Thus $(\varphi_t, \dot{\varphi}_t)$ is a solution of the control system so that, $\mathcal{V}_t$ drives the system from $(\widetilde{\mathbf{q}}_0, \widetilde{\mathbf{p}}_0)$ to $(\widetilde{\mathbf{q}}_t, \widetilde{\mathbf{p}}_t)$. We let $\mathcal{A}_t(\widetilde{\mathbf{q}}_0, \widetilde{\mathbf{p}}_0)$ denote the set of accessible points starting from $(\widetilde{\mathbf{q}}_0, \widetilde{\mathbf{p}}_0)$ at time $t$, and using the control above we have $\mathcal{A}_t(\widetilde{\mathbf{q}}_0, \widetilde{\mathbf{p}}_0) = \widehat{\mathcal{L}}_t^d \times \mathbb{R}^{3d}$. Since, by [4, Corollary 6.2], the support of the transition kernel is equal to the closure in the uniform topology of $\mathcal{A}_t(\widetilde{\mathbf{q}}_0, \widetilde{\mathbf{p}}_0)$, it follows that the transition kernel is positive. □

Now, let us denote $\mathcal{B}_\delta(x)$ the open ball of radius $\delta$ centered at $x$. We fix the domain at the initial position $\mathcal{L}_0$, and summarize the results of this section in the following Corollary:

**Corollary 2.** *At time $t_k = kT$, the transition kernel*

$$\widehat{\mathcal{P}}_{t_k,0}(\mathbf{y}, \overline{B}),\ \overline{B} \in \mathcal{B}(\mathcal{L}_0^d \times \mathbb{R}^{3d}),\ \mathbf{y} = \mathbf{x}_0,$$

*satisfies, for some fixed compact set $C \in \mathcal{B}(\mathcal{L}_0^d \times \mathbb{R}^{3d})$, the following:*

- *for some $z^* \in int(C)$ there exists $\delta > 0$, such that*

$$\widehat{\mathcal{P}}_{t_k,0}(\mathbf{y}, \mathcal{B}_\delta(z^*)) > 0, \quad \forall \widehat{\mathbf{x}} \in C$$

- *for $t_k$, the transition kernel possesses a density $\widehat{\psi}(\widehat{\mathbf{x}}, \widehat{\mathbf{y}})$ precisely*

$$\widehat{\mathcal{P}}_{t_k,0}(\mathbf{y}, \overline{B}) = \int_{\overline{B}} \widehat{\psi}(\widehat{\mathbf{x}}, \widehat{\mathbf{y}}) d\widehat{\mathbf{y}},\ \forall \widehat{\mathbf{x}}_k \in C,\ \overline{B} \in \mathcal{B}(\widehat{\mathcal{L}}_t^d \times \mathbb{R}^{3d}) \cap \mathcal{B}(C),$$

  *and $\widehat{\psi}(\widehat{\mathbf{x}}, \widehat{\mathbf{y}})$ is jointly continuous in $(\widehat{\mathbf{x}}, \widehat{\mathbf{y}}) \in C \times C$.*

*Proof.* The proof of the first argument relies on the positivity of the transition kernel as proven in Lemma 12, while the second argument is based on the smoothness of the density demonstrated in Lemma 11. □

We use Corollary 2 in the next section to show that the Lyapunov function satisfies the minorization condition.

### 2.4.4 Markov Process Convergence

We show in this section that the Markov process $\widehat{\mathbf{X}}_t$ converges to a measure on $\widehat{\mathcal{L}}_t^d \times \mathbb{R}^{3d}$.

Let us denote by $(Q_k = \widehat{\mathbf{q}}_{kT}, P_k = \widehat{\mathbf{p}}_{kT}) \in \mathcal{L}_0^d \times \mathbb{R}^{3d}$, a discrete Markov chain constructed from the particle coordinates at the start of each period, where $\widehat{\mathbf{X}}_0 = (Q_0, P_0)$ is the initial coordinate of the time-inhomogeneous process $(\widehat{\mathbf{q}}_t, \widehat{\mathbf{p}}_t)$. Then, we define

$$(\mathcal{G}_T \mathbf{f})(Q_k, P_k) = \mathbb{E}\Big(\mathbf{f}(Q_{k+1}, P_{k+1})|(Q_k, P_k)\Big),$$

the discrete generator of the Markov chain. In addition, we consider the Lyapunov function

$$\mathcal{K}_n(\widehat{\mathbf{q}}, \widehat{\mathbf{p}}) = 1 + \|\widehat{\mathbf{p}}\|^{2n}, n \geq 1 \tag{2.17}$$

with the associated weighted $L^\infty$ norms defined by

$$\|\mathbf{h}\|_{L^\infty_{\mathcal{K}_n}} = \left\| \frac{\mathbf{h}}{\mathcal{K}_n} \right\|_{L^\infty}.$$

We begin by demonstrating that the discrete process converges exponentially to an invariant measure, and then we use this result to prove that the continuous process also converges to a measure.

#### 2.4.4.1 The Invariant Measure of the Discrete Process

The convergence of the Markov chain $\big(Q_{k+1}, P_{k+1}\big)$ is based on the uniform Lyapunov condition [20, Assumpion 1] and the uniform minorization condition [20, Assumpion 2] that we prove in the following two Lemmas.

**Lemma 13.** *(Uniform Lyapunov condition) There exists $a_n \in [0,1)$ and $b_n > 0$ such that*

$$\mathcal{G}_T \mathcal{K}_n \leq a_n \mathcal{K}_n + b_n, \tag{2.18}$$

*for $\mathcal{K}_n$ defined in* (2.17)*.*

*Proof.* Using the Itô's lemma, we get

$$d\mathbf{f}(\widehat{\mathbf{X}}_t) = \big(G\mathbf{f}\big)(\widehat{\mathbf{X}}_t)dt + \Big\langle \nabla \mathbf{f}(\widehat{\mathbf{X}}_t), \widehat{\Sigma} dW \Big\rangle,$$

where

$$G = \langle \widehat{\mathbf{p}} + A\widehat{\mathbf{q}}, \nabla_{\widehat{\mathbf{q}}} \cdot \rangle + \langle -\nabla V(\widehat{\mathbf{q}}), \nabla_{\widehat{\mathbf{p}}} \cdot \rangle - \gamma \langle \widehat{\mathbf{p}}, \nabla_{\widehat{\mathbf{p}}} \cdot \rangle + \frac{1}{2}\sigma\sigma^T : \nabla^2.$$

Then, it follows that

$$\begin{aligned} G\mathcal{K}_n(\widehat{\mathbf{q}}, \widehat{\mathbf{p}}) =& - n \left\|\widehat{\mathbf{p}}\right\|_2^{n-2} \langle \nabla V(\widehat{\mathbf{q}}), \widehat{\mathbf{p}} \rangle - n\gamma \Big( \langle \widehat{\mathbf{p}}, \widehat{\mathbf{p}} \rangle - \frac{n+d-2}{\beta} \Big) \left\|\widehat{\mathbf{p}}\right\|_2^{n-2} \\ \leq& - n\gamma \left\|\widehat{\mathbf{p}}\right\|_2^n + n \left\|\nabla V(\widehat{\mathbf{q}})\right\|_2 \left\|\widehat{\mathbf{p}}\right\|_2^{n-1} + n\gamma \frac{n+d-2}{\beta} \left\|\widehat{\mathbf{p}}\right\|_2^{n-2}. \end{aligned}$$

Thus, there exists $\widehat{a}_n, \widehat{b}_n \geq 0$ such that

$$G\mathcal{K}_n \leq -\widehat{a}_n \mathcal{K}_n + \widehat{b}_n, \quad \widehat{a}_n = n\gamma/2, \quad \text{as } \lim_{|\widehat{\mathbf{q}}, \widehat{\mathbf{p}}| \to \infty} \frac{G\mathcal{K}_n}{\mathcal{K}_n} \leq -\widehat{a}_n,$$

and it follows that

$$d\mathcal{K}_n(\widehat{\mathbf{X}}_t) \leq (-\widehat{a}_n\mathcal{K}_n + \widehat{b}_n)dt + \left\langle \nabla\mathcal{K}_n(\widehat{\mathbf{X}}_t), \widehat{\Sigma}dW \right\rangle.$$

Using Grönwall's inequality, we have the desired result

$$\mathbb{E}[\mathcal{K}_n(Q_{k+1}, P_{k+1})] \leq e^{-\widehat{a}_n T}\mathcal{K}_n(Q_k, P_k) + \frac{\widehat{b}_n}{\widehat{a}_n}\Big(1 - e^{-\widehat{a}_n\theta}\Big) \leq e^{-\widehat{a}_n T}\mathcal{K}_n(Q_k, P_k) + \frac{\widehat{b}_n}{\widehat{a}_n}.$$

□

**Lemma 14.** *(Uniform minorization condition) Fix any $p_{max} > 0$, then there exists a probability measure $\vartheta : \mathcal{L}_0^d \times \mathbb{R}^{3d} \to \mathbb{R}$ and a constant $\kappa$ such that,*

$$\forall \overline{B} \in \mathcal{B}(\mathcal{L}_0^d \times \mathbb{R}^{3d}), \quad \mathbb{P}\Big((Q_{k+1}, P_{k+1}) \in \overline{B} \;\Big|\; \|P_k\|_2 \leq p_{max}\Big) \geq \kappa\vartheta(\overline{B}).$$

The proof is essentially based on the arguments from [4, 37] which uses the continuity property of the Markov process, the regularity of the transition kernel. Before we start the proof, we consider the following Lemma:

**Lemma 15.** *[37, Lemma 2.3] If the Markov chain $(Q_k, P_k)$ satisfies the assumption in Corollary 2, then there is a choice of time $t_k = kT$, $\kappa \geq 0$, a probability measure $\vartheta$, with $\vartheta(C^c) = 0$ and $\vartheta(C) = 1$, such that*

$$\overline{\mathcal{P}}_{t_k,0}(\mathbf{y}, \overline{B}) \geq \kappa\vartheta(\overline{B}), \quad \forall \overline{B} \in \mathcal{B}(\mathcal{L}_0^d \times \mathbb{R}^{3d}),\ \mathbf{y} \in C. \tag{2.19}$$

The proof of Lemma 14 follows from the fact that the discrete chain $(Q_{k+1}, P_{k+1}) \in \overline{B}$ satisfies the assumption in Corollary 2. By using the above Lemma, we can deduce the desired result.

Using the previous Lemmas, we state the following uniform convergence result for the sampled chain $(Q_k, P_k)$ from [20]:

**Theorem 16.** *[20, Theorem 1.2] If $\mathcal{G}_T$ satisfies the Lyapunov condition as in Lemma 13 and the minorization condition as in Lemma 14, then there exists an invariant measure $\pi_0$ and constants $C_n, \lambda_n > 0$ for any $n \geq 1$ such that*

$$\left\| \mathcal{G}_T^k \mathbf{f} - \overline{\mathbf{f}} \right\|_{L^\infty_{\mathcal{K}_n}} \leq C_n e^{-k\lambda_n T} \left\| \mathbf{f} - \overline{\mathbf{f}} \right\|_{L^\infty_{\mathcal{K}_n}}, \quad \forall k \geq 0, \tag{2.20}$$

*where*

$$\overline{\mathbf{f}} = \int_{\mathcal{L}_0^d \times \mathbb{R}^{3d}} \mathbf{f}(\widehat{\mathbf{q}}, \widehat{\mathbf{p}}) \pi_0(\widehat{\mathbf{q}}, \widehat{\mathbf{p}}) d\widehat{\mathbf{q}} d\widehat{\mathbf{p}}.$$

Then, we derive the convergence of the continuous process $(\widehat{\mathbf{q}}_t, \widehat{\mathbf{p}}_t)$ in the following Lemma:

**Proposition 1.** *The Markov process $(\widehat{\mathbf{q}}_t, \widehat{\mathbf{p}}_t)$ converges exponentially to the limit cycle $\pi_\theta$:*

$$\left| \mathbb{E}^{s,\mathbf{y}}[\mathbf{f}(\widehat{\mathbf{X}}_t)] - \overline{\mathbf{f}}([t]) \right| \leq C_n e^{-\lambda_n t} \left\| \mathbf{f} - \overline{\mathbf{f}}([t]) \right\|_{L^\infty_{\mathcal{K}_n}} \Big( 1 + \mathcal{K}_n(\mathbf{y}) \Big), \quad \mathbf{y} = \widehat{\mathbf{X}}_0,$$

*where* $\overline{\mathbf{f}}([t])$ *is defined as*

$$\overline{\mathbf{f}}(\theta) = \int_{\widehat{\mathcal{L}}_\theta^d \times \mathbb{R}^{3d}} \mathbf{f}_\theta(\widehat{\mathbf{q}}, \widehat{\mathbf{p}}) \pi_\theta(\widehat{\mathbf{q}}, \widehat{\mathbf{p}}) d\widehat{\mathbf{q}} d\widehat{\mathbf{p}}. \tag{2.21}$$

*Proof.* We use an argument from [42, 37] and the result from Theorem 16 to show that the Markov process $(\widehat{\mathbf{q}}_t, \widehat{\mathbf{p}}_t) \in \widehat{\mathcal{L}}_t^d \times \mathbb{R}^{3d}$ converges exponentially to the limit cycle $\pi_\theta$. We start by using the result from Lemma 13 and Lemma 14, and derive from Theorem 16 that

$$\begin{aligned} \left| \mathbb{E}^{0,\mathbf{y}}[\mathbf{f}(\widehat{\mathbf{X}}_{kT})] - \overline{\mathbf{f}} \right| &\leq C_n e^{-\lambda_n kT} \left\| \mathbf{f} - \overline{\mathbf{f}} \right\|_{L^\infty_{\mathcal{K}_n}} \mathcal{K}_n(\mathbf{y}), \\ \overline{\mathbf{f}} &= \int_{\mathcal{L}_0^d \times \mathbb{R}^{3d}} \mathbf{f}(\widehat{\mathbf{q}}, \widehat{\mathbf{p}}) \pi_0(\widehat{\mathbf{q}}, \widehat{\mathbf{p}}) d\widehat{\mathbf{q}} d\widehat{\mathbf{p}}. \end{aligned}$$

Further, we have

$$\left| \mathbb{E}^{0,\mathbf{y}}[\mathbf{f}(\widehat{\mathbf{X}}_{kT+\theta})] - \overline{\mathbf{f}}(\theta) \right| \leq C_n e^{-\lambda_n kT} \left\| \mathbf{f} - \overline{\mathbf{f}}(\theta) \right\|_{L^\infty_{\mathcal{K}_n}} \mathbb{E}^{0,\mathbf{y}}[\mathcal{K}_n(\widehat{\mathbf{X}}_\theta)]. \tag{2.22}$$

We compute an upper bound on $\mathbb{E}^{0,\mathbf{y}}[\mathcal{K}_n(\widehat{\mathbf{X}}_\theta)]$ as follows: Then, we get an upper bound on $\mathbb{E}^{0,\mathbf{y}}[\mathcal{K}_n(\widehat{\mathbf{x}}_\theta)]$ by using Grönwall's inequality:

$$\mathbb{E}^{0,\mathbf{y}}[\mathcal{K}_n(\widehat{\mathbf{X}}_\theta)] \leq e^{-\widehat{a}_n \theta} \mathcal{K}_n(\mathbf{y}) + \frac{\widehat{b}_n}{\widehat{a}_n} \Big( 1 - e^{-\widehat{a}_n \theta} \Big) \leq e^{-\widehat{a}_n \theta} \mathcal{K}_n(\mathbf{y}) + \frac{\widehat{b}_n}{\widehat{a}_n}.$$

Plugging the latter result in (2.22), we have

$$\left| \mathbb{E}^{0,\mathbf{y}}[\mathbf{f}(\widehat{\mathbf{X}}_{kT+\theta})] - \overline{\mathbf{f}}(\theta) \right| \leq C_n e^{-\lambda_n kT} \left\| \mathbf{f} - \overline{\mathbf{f}}(\theta) \right\|_{L^\infty_{\mathcal{K}_n}} \Big( e^{-\widehat{a}_n \theta} \mathcal{K}_n(\mathbf{y}) + \frac{\widehat{b}_n}{\widehat{a}_n} \Big).$$

Defining $\lambda_n$ by $e^{-\lambda_n} = \widehat{a}_n^{\frac{1}{T}}$, we obtain the expected result by redefining $C_n \to \Big(1 + \frac{\widehat{b}_n}{\widehat{a}_n} e^{\lambda_n T}\Big)$:

$$\Big|\mathbb{E}^{0,\mathbf{y}}[\mathbf{f}(\widehat{\mathbf{X}}_{kT+\theta})] - \overline{\mathbf{f}}(\theta)\Big| \leq C_n e^{-\lambda_n(kT+\theta)} \left\|\mathbf{f} - \overline{\mathbf{f}}(\theta)\right\|_{L^\infty_{\mathcal{K}_n}} \Big(1 + \mathcal{K}_n(\mathbf{y})\Big).$$

□

#### 2.4.4.2 Convergence in Law of Large Numbers for $\big(\widehat{\mathbf{q}}_{kT+\theta}, \widehat{\mathbf{p}}_{kT+\theta}\big)$

We use Lemmas from the previous section and mainly [41] to show that $\big(\widehat{\mathbf{q}}_{kT+\theta}, \widehat{\mathbf{p}}_{kT+\theta}\big)$ is a positive Harris recurrent chain. Thus, the Law of Large Number holds:

**Proposition 2.** *(Law of Large Numbers for the sampled chain) For any* $\mathbf{f} \in L^\infty_{\mathcal{K}_n}$,

$$\frac{1}{N}\sum_{k=1}^{N} \mathbf{f}(\widehat{\mathbf{q}}_{kT+\theta}, \widehat{\mathbf{p}}_{kT+\theta}) \xrightarrow[N\to+\infty]{} \int_{\mathcal{L}^d_\theta \times \mathbb{R}^{3d}} \mathbf{f}(\widehat{\mathbf{q}}, \widehat{\mathbf{p}}) \nu(\widehat{\mathbf{q}}, \widehat{\mathbf{p}}) d\widehat{\mathbf{q}} d\widehat{\mathbf{p}} \quad a,s.\ , \tag{2.23}$$

*for all the initial conditions* $(Q_0, P_0)$.

*Proof.* Since $\big(\widehat{\mathbf{q}}_{kT+\theta}, \widehat{\mathbf{p}}_{kT+\theta}\big)$ is regularized for all $\theta \in T\mathbb{T}$, showing that the Law of Large Numbers converges for the Markov chain $(Q_k, P_k) \in \mathcal{L}^d_0 \times \mathbb{R}^{3d}$ when $\theta = 0$ is sufficient to establish the validity of (2.23) for all $\theta \in T\mathbb{T}$. Corollary 2 from the previous Section shows that the chain $\big(Q_k, P_k\big)$ is irreducible with respect to the Lebesgue measure. Thus, the result from [58, Corollary 1] based on [41, Page 199] provides that the chain $\big(Q_k, P_k\big)$ is Harris recurrent. In addition as $\nu(t, \widehat{\mathbf{q}}, \widehat{\mathbf{p}})$ is positive using Lemma 12, it follows from [41, Theorem 17.0.1] that the Law of Large Numbers holds. □

## 2.5 Conclusion

In this paper, we study the ergodicity of NELD under shear flow and planar elongational flow using respectively LE and KR Periodic boundary conditions. This is essentially formulated in Proposition 1 where, after showing existence and uniqueness of the limit cycle using a Lyapunov function and a minorization condition, we established the exponential convergence of the Markov chain generated by the NELD equation given all the initial conditions. It will be interesting to establish the convergence analysis for the three dimensional diagonalizable incompressible flow cases using the R-KR [13] algorithm or the GenKR [10, 24] algorithm. However additional analysis will be needed since these PBCs have geometry that is not as simple as the current case studied.

# CHAPTER 3

# STRONG CONVERGENCE OF INTEGRATORS FOR NONEQUILIBRIUM LANGEVIN DYNAMICS

**Note.** This chapter is published and cited as: *"Strong convergence of integrators for nonequilibrium Langevin dynamics", by Matthew Dobson and Abdel Kader A. Geraldo in 2019, Molecular Simulation, 45:11, pp. 912-920, doi.org/10.1080/08927022.2019.1610950*

## 3.1 Abstract

Several numerical schemes are proposed for the solution of Nonequilibrium Langevin Dynamics (NELD), and the strong rate of convergence for each scheme is analyzed. The schemes considered here employ specialized periodic boundary conditions that deform with the flow, namely Lees-Edwards, and Kraynik-Reinelt boundary conditions and their generalizations. We show that care must be taken when implementing standard stochastic integration schemes with these boundary conditions in order to avoid a breakdown in the strong order of convergence.

## 3.2 Introduction

Nonequilibrium molecular dynamics techniques have been widely employed in the study of rheological properties of dense microscopic fluids under background flow con-

ditions such as steady shear or elongational flow [17, 62]. We consider the study of dense solutions of complex particles with a time-independent, spatially varying background flow. These computations are used to study the bulk rheological properties of both simple and complex fluids such as in the study of polymer melts [51]. The existence of a steady-state, spatially varying flow requires some form of driving terms, and a wide range of dynamics have been proposed for such simulations including the deterministic SLLOD dynamics [22, 16, 17] and generalizations of Langevin dynamics which we denote here as Nonequilibrium Langevin Dynamics (NELD) [38, 54, 14]. The study of bulk properties of dense systems at nonequilibrium also requires the application of specialized periodic boundary conditions (PBCs) that are compatible with the steady flow, notably the Lees-Edwards boundary conditions, Kraynik-Reinelt boundary conditions, or their generalizations [28, 61, 10, 24]. In this work, we examine the strong rate of convergence of several numerical integrators for the NELD equations of motion and show how this rate is affected by the interaction with the boundary conditions.

A closely related class of schemes for studying polymer flows are the Brownian Dynamics (BD) methods [15, 50, 5], whose key modeling assumption is that the large particles have their velocities reach equilibrium much faster than the particles move, thus giving the regime of overdamped Langevin dynamics. BD methods have been typically used for dilute polymer fluids, studying the conformational properties of a single large polymer under extensional and shear flows, with implicitly-modeled hydrodynamic interactions and wide range of coarse-grained interaction laws [1, 43]. When studying single polymer systems, PBCs are not needed, so the issue of the

interaction between integrators and boundary conditions would not arise; however, recent works have implemented deforming PBCs in systems modeled with BD [55, 25].

Let $\widetilde{\mathbf{q}}, \widetilde{\mathbf{p}} \in \mathbb{R}^{3N}$ denote the positions and velocities of a set of $N$ particles, then NELD is given by

$$\begin{aligned} d\widetilde{\mathbf{q}} &= \widetilde{\mathbf{p}}\, dt \\ d\widetilde{\mathbf{p}} &= (-\nabla E(\widetilde{\mathbf{q}}) - \gamma(\widetilde{\mathbf{p}} - A\widetilde{\mathbf{q}}) + A\widetilde{\mathbf{p}})\, dt + \sigma\, dW \end{aligned} \tag{3.1}$$

where $-\nabla E(\widetilde{\mathbf{q}})$ are the interparticle forces, $A \in \mathbb{R}^{3N\times 3N}$ is trace-free block diagonal linear background flow matrix $W$ is a standard $3N$-dimensional Brownian motion whose components are independent, and $\sigma$ and $\gamma$ are scalar constants satisfying the fluctuation-dissipation relation

$$\gamma = \frac{1}{2}\sigma^2\beta \tag{3.2}$$

where $\beta = \frac{1}{k_B T}$ is the inverse temperature. The diagonal entries of $A$ are identical $3 \times 3$ trace-free diagonal matrices, corresponding to the macroscale background flow $A = \nabla \mathbf{u}$. The two terms in NELD that do not appear in equilibrium Langevin dynamics

$$\begin{aligned} d\widetilde{\mathbf{q}} &= \widetilde{\mathbf{p}}\, dt \\ d\widetilde{\mathbf{p}} &= (-\nabla E(\widetilde{\mathbf{q}}) - \gamma\widetilde{\mathbf{p}})\, dt + \sigma\, dW \end{aligned} \tag{3.3}$$

both drive the system to move with the background flow. The dissipation $-\gamma(\widetilde{\mathbf{p}} - A\widetilde{\mathbf{q}})$ is applied to the peculiar velocity $\widehat{\mathbf{p}} = \widetilde{\mathbf{p}} - A\widetilde{\mathbf{q}}$, that is, it is relative to the background

flow. The term $A\widetilde{\mathbf{p}}$ is an additional driving force from the background flow that is consistent with the periodic boundary conditions described below. The NELD equations of motions were derived using a Mori-Zwanzig argument on the peculiar velocities in [38], where the peculiar velocity $\widehat{\mathbf{p}} = \widetilde{\mathbf{p}} - A\widetilde{\mathbf{q}}$ satisfies the equilibrium Langevin dynamics $d\widehat{\mathbf{p}} = (-\nabla E(\widetilde{\mathbf{q}}) - \gamma\widehat{\mathbf{p}})\,dt + \sigma\,dW$. It has also been derived micromechanical model in [14].

To simulate the bulk motion of particles with a mean background flow $A$, specialised periodic boundary conditions are employed where the simulation box deforms with the flow. A particle with the coordinates $(\widetilde{\mathbf{q}}, \widetilde{\mathbf{p}})$ has periodic images at $(\widetilde{\mathbf{q}} + L_t\mathbf{n}, \widetilde{\mathbf{p}} + AL_t\mathbf{n})$, where $L_t : [0, \infty) \to \mathbb{R}^{3N\times 3N}$ is a block diagonal matrix whose identical $3 \times 3$ blocks denote the matrix of lattice basis vectors at time $t$ and $\mathbf{n} \in \mathbb{Z}^{3N}$. Unlike equilibrium periodic boundary conditions, the particle images do not have the same velocity. This in turn implies that the periodic lattice generated by $L_t$ deforms with the flow,

$$\frac{d}{dt}(\widetilde{\mathbf{q}} + L_t\mathbf{n}) = \widetilde{\mathbf{p}} + AL_t\mathbf{n} \text{ for all } \mathbf{n} \in \mathbb{Z}^{3N} \implies \frac{d}{dt}L_t = AL_t.$$

Care is needed to ensure that the lattice does not become degenerately deformed where the minimum image distance goes to zero. For example, if a system under elongational flow has a simulation box with sides parallel to the compressive direction, then the distance between particle images will decay exponentially. Techniques have been developed [31, 28, 10, 24] which choose initial lattice vectors $L_0$ such that the minimum image distance in the lattice stays bounded away from zero, and the simulation box is remapped so that the geometry stays regular. We will consider

the Generalised Kraynik-Reinelt (GenKR) boundary conditions developed in [10, 24], which can handle general three-dimensional incompressible flows.

In this paper, we will focus on the strong convergence properties of certain common stochastic integrators applied to NELD, seeing how the periodic boundary conditions interact with the convergence. Strong convergence is a common convergence criteria that is important when one wants to have accurate dynamical trajectories in the simulation. From a sampling standpoint, it is more common to look at the sampling bias due to errors of the invariant measure for the integrator; however, unlike the equilibrium Langevin case, the invariant measure for NELD with deforming boundary conditions is not known analytically. We hope to analyze the errors in sampling due to the invariant measure in future work. We adapt the standard approach of computing the truncation error via Ito-Taylor expansions [27, 53] to the nonequilibrium case. The novelty in our analysis is the treatment of the interaction of the stochastic integrators with the remapping of the simulation box inherent in the periodic boundary conditions used. In particular, we see that a naive implementation of certain standard schemes exhibits a breakdown in convergence. We then develop schemes that avoid this convergence problems and compute the order of convergence by using the Ito-Taylor expansion. Several standard first and second order schemes are demonstrated numerically and analytically.

## 3.3 Ito-Taylor expansion of the nonequilibrium Langevin dynamics

In this section, we compute the Ito-Taylor expansion for the NELD up to second order, which will be used in the error analysis of the numerical integrators. We also set the notation for the application of boundary conditions as the motion of the image particles plays an important role in the analysis of the numerical schemes.

### 3.3.1 Review of the Ito-Taylor expansion

We express the NELD (3.1) in integral form,

$$X(t) = X(t_0) + \int_{t_0}^{t} \mathrm{C}(X(s))\, ds + \int_{t_0}^{t} \Sigma\, dW(s) \tag{3.4}$$

where

$$X = \begin{bmatrix} \widetilde{\mathbf{q}} \\ \widetilde{\mathbf{p}} \end{bmatrix}, \quad C\left(\begin{bmatrix} \widetilde{\mathbf{q}} \\ \widetilde{\mathbf{p}} \end{bmatrix}\right) = \begin{bmatrix} \widetilde{\mathbf{p}} \\ -\nabla E(\widetilde{\mathbf{q}}) - \gamma(\widetilde{\mathbf{p}} - A\widetilde{\mathbf{q}}) + A\widetilde{\mathbf{p}} \end{bmatrix}, \text{ and } \quad \Sigma = \begin{bmatrix} 0 & 0 \\ 0 & \sigma I \end{bmatrix}.$$

The Ito formula for a scalar-valued function $G(X(t))$ of the solution $X(t)$ is given by

$$G(X(t)) = G(X(t_0)) + \int_{t_0}^{t} L^0 G(X(s))\, ds + \int_{t_0}^{t} L^1 G(X(s))\, dW(s) \tag{3.5}$$

where the operators $L^0$ and $L^1$ are given by

$$L^0 = \mathrm{C} \cdot \nabla_x + \frac{1}{2}\Sigma\Sigma^T : \nabla_x^2, \quad L^1 = \Sigma \nabla_x\,, \tag{3.6}$$

where we recall the notation

$$\begin{aligned} \mathrm{C}\cdot\nabla_x = \sum_{j=1}^{6N} C_j \frac{\partial}{\partial x_j}, \quad \Sigma\Sigma^T : \nabla_x^2 = \sum_{i=1}^{6N}\sum_{j=1}^{6N} \Sigma_{ij}\Sigma_{ji}\frac{\partial^2}{\partial x_i \partial x_j}, \\ (\Sigma\nabla_x)_i = \sum_{j=1}^{6N} \Sigma_{ij}\frac{\partial}{\partial x_j}\,. \end{aligned} \tag{3.7}$$

We apply the Ito formula twice in equation (3.4), arriving at

$$\begin{aligned} X(t) = X(t_0) &+ \int_{t_0}^{t} \mathrm{C}(X(t_0))\,ds + \int_{t_0}^{t} \Sigma\,dW(s) \\ &+ \int_{t_0}^{t}\int_{t_0}^{s} L^0\mathrm{C}(X(t_0))\,du\,ds \\ &+ \int_{t_0}^{t}\int_{t_0}^{s} L^1\mathrm{C}(X(t_0))\,dW(u)\,ds \\ &+ \int_{t_0}^{t}\int_{t_0}^{s}\int_{t_0}^{u} L^1L^0C(X(v))\,dW(v)\,du\,ds \\ &+ \int_{t_0}^{t}\int_{t_0}^{s}\int_{t_0}^{u} L^0L^0C(X(v))\,dv\,du\,ds \\ &+ \int_{t_0}^{t}\int_{t_0}^{s}\int_{t_0}^{u} L^1L^1C(X(v))\,dW(v)\,dW(u)\,ds \\ &+ \int_{t_0}^{t}\int_{t_0}^{s}\int_{t_0}^{u} L^0L^1C(X(v))\,dv\,dW(u)\,ds. \end{aligned} \tag{3.8}$$

Since $\widetilde{\mathbf{p}}$ appears in $C(X)$ only in linear terms, we have that $L^0L^1C(X) = 0$ and $L^1L^1C(X) = 0$. For a small time interval $\Delta t = t - t_0$, we have

$$\begin{aligned} X(t) = X(t_0) + \Delta t\,\mathrm{C}(X(t_0)) + \Sigma(W(t) - W(t_0)) + \frac{\Delta t^2}{2}L^0\mathrm{C}(X(t_0)) \\ + L^1\mathrm{C}(X(t_0))\int_{t_0}^{t} W(s) - W(t_0)\,ds + R, \end{aligned} \tag{3.9}$$

where the remainder term, which is $\mathrm{O}(\Delta t^{5/2})$, is given by

$$\begin{aligned} R = &\int_{t_0}^{t}\int_{t_0}^{s}\int_{t_0}^{u} L^1 L^0 C(X(v))\, dW(v)\, du\, ds \\ &+ \int_{t_0}^{t}\int_{t_0}^{s}\int_{t_0}^{u} L^0 L^0 C(X(v))\, dv\, du\, ds. \end{aligned} \tag{3.10}$$

We recall the following facts about the covariance of $W(t)$ and its integral, which are useful in developing numerical schemes [63, 27]:

$$\begin{aligned} \mathbb{E}(W_i(s)W_j(t)) &= \delta_{ij}\min(s,t), \\ \mathbb{E}[(W_i(t+\Delta t) - W_i(t))(W_j(t+\Delta t) - W_j(t))] &= \delta_{ij}\Delta t, \\ \mathbb{E}\left[(W_i(t+\Delta t) - W_i(t))\int_t^{t+\Delta t}(W_j(s) - W_j(t))\, ds\right] &= \frac{1}{2}\delta_{ij}\Delta t^2, \\ \mathbb{E}\left[\int_t^{t+\Delta t}(W_i(s) - W_i(t))\, ds \int_t^{t+\Delta t}(W_j(s) - W_j(t))\, ds\right] &= \frac{1}{3}\delta_{ij}\Delta t^3. \end{aligned} \tag{3.11}$$

Using the above variances and covariances we define the following independent Gaussian increments

$$\begin{aligned} \boldsymbol{\xi}(t) &= \frac{W(t) - W(t_0)}{\Delta t^{1/2}}, \\ \boldsymbol{\eta}(t) &= \frac{2\sqrt{3}}{\Delta t^{3/2}}\int_{t_0}^{t}(W(s) - W(t_0))\; ds \;-\; \sqrt{3}\,\boldsymbol{\xi}(t). \end{aligned}$$

The scaling of stochastic terms has been chosen so that $\boldsymbol{\xi}, \boldsymbol{\eta} \sim \mathcal{N}(0, I_{3N})$ are independent Gaussian random variables. Therefore, truncating the expansion of NELD to second order and letting $(\widetilde{\mathbf{q}}, \widetilde{\mathbf{p}})$ denote the coordinates at time $t_0$, we arrive at

$$\begin{aligned}\begin{bmatrix}\widetilde{\mathbf{q}}(t)\\ \widetilde{\mathbf{p}}(t)\end{bmatrix} &= \begin{bmatrix}\widetilde{\mathbf{q}}\\ \widetilde{\mathbf{p}}\end{bmatrix} + \Delta t \begin{bmatrix}\widetilde{\mathbf{p}}\\ \mathrm{F}(\widetilde{\mathbf{p}},\widetilde{\mathbf{q}})\end{bmatrix} + \Delta t^{1/2}\begin{bmatrix}0 & 0\\ 0 & \sigma I\end{bmatrix}\boldsymbol{\xi}(t)\\ &\quad + \frac{\Delta t^2}{2}\begin{bmatrix}\mathrm{F}(\widetilde{\mathbf{p}},\widetilde{\mathbf{q}})\\ (-\nabla^2 E(\widetilde{\mathbf{q}}) + \gamma A)\widetilde{\mathbf{p}} + (A-\gamma I)\mathrm{F}(\widetilde{\mathbf{p}},\widetilde{\mathbf{q}})\end{bmatrix}\\ &\quad + \sigma\Delta t^{\frac{3}{2}}\begin{bmatrix}0 & I\\ 0 & (A-\gamma I)\end{bmatrix}\left(\frac{1}{2}\boldsymbol{\xi}(t) + \frac{1}{2\sqrt{3}}\boldsymbol{\eta}(t)\right) + \mathrm{O}(\Delta t^{\frac{5}{2}}),\end{aligned} \tag{3.12}$$

where

$$\mathrm{F}(\widetilde{\mathbf{p}},\widetilde{\mathbf{q}}) = -\nabla E(\widetilde{\mathbf{q}}) - \gamma(\widetilde{\mathbf{p}} - A\widetilde{\mathbf{q}}) + A\widetilde{\mathbf{p}}. \tag{3.13}$$

### 3.3.2 Nonequilibrium Boundary Conditions

When analyzing the truncation error for the scheme, it is important to account for the nonequilibrium periodic boundary conditions, particularly the fact that particle images do not all have the same velocity. A particle with coordinates $(\widetilde{\mathbf{q}},\widetilde{\mathbf{p}})$ has periodic images at $(\widetilde{\mathbf{q}} + L_t\mathbf{n}, \widetilde{\mathbf{p}} + AL_t\mathbf{n})$. The NELD equations are invariant under a translation of the system by choosing new $\mathbf{n}$. In particular, $d\widetilde{\mathbf{q}} = \widetilde{\mathbf{p}}\,dt$ holds for all particle images, so that

$$\frac{d}{dt}(\widetilde{\mathbf{q}} + L_t\mathbf{n}) = \widetilde{\mathbf{p}} + AL_t\mathbf{n},$$

which implies that the simulation box deforms with the flow, $\frac{d}{dt}L_t = AL_t$ with a solution $L_t = \exp(At)L_0$.

During a simulation step, one or more particles can leave the simulation box, whereupon they are remapped in accordance to the periodic boundary conditions. This can also be viewed as no longer tracking the position of the particles that started

at $(\widetilde{\mathbf{q}}, \widetilde{\mathbf{p}})$, but tracking the particles at $(\widetilde{\mathbf{q}} + L_t\mathbf{n}, \widetilde{\mathbf{p}} + AL_t\mathbf{n})$ for some $\mathbf{n} \in \mathbb{Z}^{3N}$. We show in the following that the timing of applying the periodic boundary conditions affects the rate of convergence for the numerical scheme, in fact, reducing the strong rate of convergence below first order for a pair of schemes. When computing the local truncation error, we compare the final position after the numerical step and periodic remapping with the Taylor-Ito expansion of the corresponding image, which may have started outside the simulation box. That is, if we are now tracking the particle at $(\widetilde{\mathbf{q}}(t) + L_t\mathbf{n}, \widetilde{\mathbf{p}}(t) + AL_t\mathbf{n})$, we compare with the particle that started at $(\widetilde{\mathbf{q}}(t_0) + L_{t_0}\mathbf{n}, \widetilde{\mathbf{p}}(t_0) + AL_{t_0}\mathbf{n})$. We note that the Taylor-Ito expansion will now have terms from the deformed lattice vectors,

$$\widetilde{\mathbf{q}}(t) + L_t\mathbf{n} = \widetilde{\mathbf{q}}(t) + L_{t_0}\mathbf{n} + \Delta t A L_{t_0}\mathbf{n} + \frac{1}{2}\Delta t^2 A^2 L_{t_0}\mathbf{n} + O(\Delta t^3),$$

with a similar expression for $\widetilde{\mathbf{p}}(t) + AL_t\mathbf{n}$.

## 3.4 Strong Convergence and Numerical Experiments

When developing integrators for an SDE, there are several notions of convergence one can consider, including strong convergence, weak convergence, or convergence of the invariant measure of the integrator to the invariant measure of the SDE. In the following, we consider strong convergence of the proposed numerical schemes. Given a stochastic process $X(t)$, we say that the numerical method generating $X_h(t)$ has strong order of convergence $r$ if

$$\mathbb{E}(|X(t) - X_h(t)|) \leq Ch^r$$

for some $C > 0$ and all sufficiently small $h > 0$.

For each of the described algorithms, we perform a benchmark test to numerically compute the strong rate of convergence. For each time, we numerically estimate the rate of convergence in the $\ell^2$ norm of both the position $\widetilde{\mathbf{q}}$ and momentum $\widetilde{\mathbf{p}}$, and in each case the convergence is observed to behave similarly in $\widetilde{\mathbf{q}}$ and $\widetilde{\mathbf{p}}$. We simulate a system of 1728 particles, having the Weeks-Chandler-Anderson (WCA) interparticle interaction potential,

$$\phi(r) = \begin{cases} \frac{1}{r^{12}} - \frac{1}{r^6} + \frac{1}{4} & r < 2^{\frac{1}{6}} \\ 0 & r \geq 2^{\frac{1}{6}}, \end{cases}$$

which is purely repulsive and continuously differentiable. The background flow used for all tests is an uniaxial extensional flow, whose diagonal blocks are given by

$$A = \begin{bmatrix} 0.2 & 0 & 0 \\ 0 & -0.1 & 0 \\ 0 & 0 & -0.1 \end{bmatrix}.$$

To compute the expected value of the error, for each numerical scheme we average 200 independent runs. Each run is initialized by first running an equilibrium simulation using standard Langevin dynamics, which acts to draw the initial condition according to the Gibbs measure corresponding to equilibrium. Then, at time zero, the background flow is turned on, so that the system evolves from the initial state according to NELD equations of motion, including deformation of the simulation box. The simulation is advanced using five different stepsizes: $\Delta t = 2.5 \times 10^{-5}, 2\Delta t, 4\Delta t, 8\Delta t$, and $16\Delta t$, where all step sizes use the same Brownian

process $W(t)$. For the finest stepsize, we use the second order scheme, SOILE-A , which is Algorithm 9, to provide a high-fidelity reference solution against which the other runs are compared. We then compute and report differences in the $\ell^2$ norm of the system, $\mathbf{e}_h(t) = \mathbb{E}\|\widetilde{\mathbf{q}}_h(t) - \widetilde{\mathbf{q}}_{fine}(t)\|_2$ and estimate the order of convergence by

$$\mathrm{ord}(t) = \frac{\log(\mathbf{e}_{2h}(t)) - \log(\mathbf{e}_h(t))}{\log 2}.$$

See [21] for an introduction to numerical computation of stochastic order of convergence.

## 3.5 Loss of Convergence Due to Boundary Interactions

We recall that the Euler-Maruyama scheme has strong order one-half when applied to stochastic equations with multiplicative noise and order one when applied to equations with additive noise, and we will show in Section 3.6 that it also has order one for the NELD case [27]. In this section, we will analyze two schemes which converge to first order when applied to equilibrium Langevin dynamics ($A = 0$), but which fail to converge to that order in the NELD case. Both schemes will be modified to have first order in Section 3.6.

### 3.5.1 Symplectic Euler A (SE-A)

For deterministic Hamiltonian dynamics, there are two types of Symplectic Euler integrators, either the position is integrated first and the momentum second as in Symplectic Euler A (SE-A) or momentum then position as in Symplectic Euler B (SE-B). For NELD with GenKR boundary conditions, we modify the SE-A scheme

by applying the PBCs at the beginning of the computation and after incrementing the position, then integrating the stochastic terms using an explicit step, as in in the Euler-Maruyama scheme. The SE-A algorithm is described as follows:

**Algorithm 3** Symplectic Euler A (SE-A)

**for** $k = 1 \dots$ Nsteps **do**
  GenKR($\widetilde{\mathbf{q}}^k, \widetilde{\mathbf{p}}^k$) ▷ Apply PBCs
  $\widetilde{\mathbf{q}}^{k+1} \leftarrow \widetilde{\mathbf{q}}^k + \Delta t \widetilde{\mathbf{p}}^k$
  GenKR($\widetilde{\mathbf{p}}^k, \widetilde{\mathbf{q}}^{k+1}$) ▷ Apply PBCs
  $\widetilde{\mathbf{p}}^{k+1} \leftarrow \widetilde{\mathbf{p}}^k + \Delta t \mathrm{F}(\widetilde{\mathbf{p}}^k, \widetilde{\mathbf{q}}^{k+1}) + \sigma \Delta t^{\frac{1}{2}} \boldsymbol{\xi}^k$

The particles are potentially remapped twice during the algorithm. We translate the pseudocode to our numerical scheme, giving

$$\begin{aligned}
\widetilde{\mathbf{q}}_1 &= \widetilde{\mathbf{q}}^k - L\mathbf{n}_1, \qquad \widetilde{\mathbf{p}}_1 = \widetilde{\mathbf{p}}^k - AL\mathbf{n}_1, \\
\widetilde{\mathbf{q}}_2 &= \widetilde{\mathbf{q}}_1 + \Delta t \widetilde{\mathbf{p}}_1, \\
\widetilde{\mathbf{q}}^{k+1} &= \widetilde{\mathbf{q}}_2 - L\tilde{\mathbf{n}}_2, \qquad \widetilde{\mathbf{p}}_2 = \widetilde{\mathbf{p}}_1 - AL\tilde{\mathbf{n}}_2, \\
\widetilde{\mathbf{p}}^{k+1} &= \widetilde{\mathbf{p}}_2 + \Delta t F(\widetilde{\mathbf{p}}_2, \widetilde{\mathbf{q}}^{k+1}) + \sigma \Delta t^{\frac{1}{2}} \boldsymbol{\xi},
\end{aligned}$$

where $F(\widetilde{\mathbf{p}}, \widetilde{\mathbf{q}}) := -\nabla E(\widetilde{\mathbf{q}}) - \gamma(\widetilde{\mathbf{p}} - A\widetilde{\mathbf{q}}) + A\widetilde{\mathbf{p}}$. Letting $\mathbf{n}_2 = \mathbf{n}_1 + \tilde{\mathbf{n}}_2$ and expanding the algorithm, we get

$$
\begin{aligned}
\begin{bmatrix} \widetilde{\mathbf{q}}^{k+1} \\ \widetilde{\mathbf{p}}^{k+1} \end{bmatrix} &= \begin{bmatrix} \widetilde{\mathbf{q}}^{k} - L\mathbf{n}_2 \\ \widetilde{\mathbf{p}}^{k} - AL\mathbf{n}_2 \end{bmatrix} \\
&\quad + \Delta t \begin{bmatrix} \widetilde{\mathbf{p}}^{k} - AL\mathbf{n}_1 \\ \Delta t \mathrm{F}(\widetilde{\mathbf{p}}^{k} - AL\mathbf{n}_2, \widetilde{\mathbf{q}}^{k} - L\mathbf{n}_2 + (\widetilde{\mathbf{p}}^{k} - AL\mathbf{n}_1)) \end{bmatrix} + \begin{bmatrix} 0 & 0 \\ 0 & \sigma I \end{bmatrix} \boldsymbol{\xi}^k \\
&= \begin{bmatrix} \widetilde{\mathbf{q}}^{k} - L\mathbf{n}_2 \\ \widetilde{\mathbf{p}}^{k} - AL\mathbf{n}_2 \end{bmatrix} + \Delta t \begin{bmatrix} \widetilde{\mathbf{p}}^{k} - AL\mathbf{n}_1 \\ \mathrm{F}(\widetilde{\mathbf{q}}^{k}, \widetilde{\mathbf{p}}^{k}) - A^2 L\mathbf{n}_2 \end{bmatrix} + \Delta t^{\frac{1}{2}} \begin{bmatrix} 0 & 0 \\ 0 & \sigma I \end{bmatrix} \boldsymbol{\xi}^k \\
&\quad + \Delta t^2 \begin{bmatrix} 0 \\ \gamma A(\widetilde{\mathbf{p}}^{k} - AL\mathbf{n}_1) - \nabla^2 E(\widetilde{\mathbf{q}}^{k})(\widetilde{\mathbf{p}}^{k} - AL\mathbf{n}_1) \end{bmatrix}.
\end{aligned} \tag{3.14}
$$

Comparing this to (3.12) applied to the image that began at $(\widetilde{\mathbf{q}}(t_0) + L_{t_0}\mathbf{n}_2, \widetilde{\mathbf{p}}(t_0) + AL_{t_0}\mathbf{n}_2)$, we find that the leading order terms in the truncation error are

$$
\begin{aligned}
T_1 &= \Delta t \begin{bmatrix} AL\tilde{\mathbf{n}}_2 \\ 0 \end{bmatrix} + \frac{\Delta t^2}{2} \begin{bmatrix} \mathrm{F}(\widetilde{\mathbf{p}}, \widetilde{\mathbf{q}}) + A^2 L\mathbf{n} \\ (\nabla^2 E(\widetilde{\mathbf{q}}) - \gamma A)(\widetilde{\mathbf{p}} - 2AL\mathbf{n}_1) + (A - \gamma I)\mathrm{F}(\widetilde{\mathbf{p}}, \widetilde{\mathbf{q}}) \end{bmatrix} \\
&\quad + \sigma \Delta t^{\frac{3}{2}} \begin{bmatrix} 0 & I \\ 0 & (A - \gamma I) \end{bmatrix} \left( \frac{1}{2}\boldsymbol{\xi}^k + \frac{1}{2\sqrt{3}}\boldsymbol{\eta}^k \right).
\end{aligned}
$$

Note that since the local truncation error contains a term of $O(\Delta t)$, we do not expect to have first-order convergence. However, this term is only non-zero when there is particle motion across the boundary, so convergence is still possible. We see in the following numerical experiment that for the chosen parameters, the order is reduced but the scheme is convergent. This term arises due to the application of periodic boundary conditions between the $\widetilde{\mathbf{q}}$ update and $\widetilde{\mathbf{p}}$ update.

### Numerical Result

Figure 3.1 plots both the errors $\mathbf{e}_h(t)$ as well as the numerically estimated order $\text{ord}_h(t)$ for the SE-A implementation. The plots show the lack of first-order convergence for the chosen parameters. We correct this problem in Section 3.6 by delaying the application of PBCs in the algorithm, arriving at the SE-AC (Symplectic Euler-A, corrected) scheme.

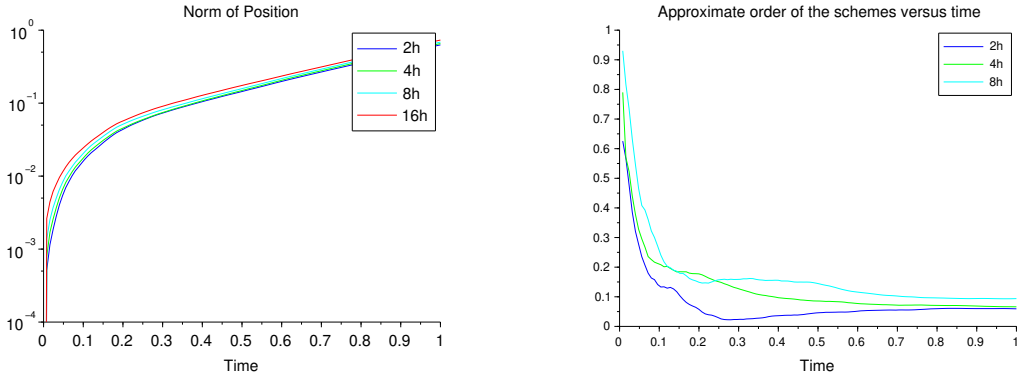


(a) (b)

**Figure 3.1:** (a) The strong error of the Symplectic Euler-A scheme for decreasing step sizes is plotted as a function of time. (b) The estimated order of convergence, which is both irregular and less than the expected order $r = 1$. A corrected version of the scheme is presented in Section 3.6.

### 3.5.2 ABAPO

We consider a splitting scheme where the Ornstein-Uhlenbeck portion is integrated analytically. We use the terminology from the framework of [32], where we split the NELD dynamics into three portions,

$$d\begin{bmatrix}\widetilde{\mathbf{q}}\\ \widetilde{\mathbf{p}}\end{bmatrix} = \underbrace{\begin{bmatrix}\widetilde{\mathbf{p}}\\ 0\end{bmatrix}dt}_{A} + \underbrace{\begin{bmatrix}0\\ -\nabla E(\widetilde{\mathbf{q}})\end{bmatrix}dt}_{B} + \underbrace{\begin{bmatrix}0\\ A\widetilde{\mathbf{p}}\end{bmatrix}dt}_{P} + \underbrace{\begin{bmatrix}0\\ -\gamma(\widetilde{\mathbf{p}} - A\widetilde{\mathbf{q}})\end{bmatrix}dt + \begin{bmatrix}0 & 0\\ 0 & \sigma I\end{bmatrix}dW}_{O}. \tag{3.15}$$

Each of these split portions can be analytically integrated, $A$, $B$, and $P$ trivially so, while the exact solution of the $O$ part is

$$\widetilde{\mathbf{p}}(t) = \exp(-\gamma\Delta t)\widetilde{\mathbf{p}}(t_0) + (1-\exp(-\gamma\Delta t))A\widetilde{\mathbf{q}}(t_0) + \sqrt{\beta^{-1}(1-\exp(-2\gamma\Delta t))}\boldsymbol{\zeta}, \tag{3.16}$$

where

$$\boldsymbol{\zeta} = \left(\frac{\beta}{1-\exp(-2\gamma\Delta t}\right)^{\frac{1}{2}} \exp(-\gamma t)\int_{t_0}^{t} \sigma\exp(\gamma s)\, dW(s) \sim \mathcal{N}(0,1).$$

We choose an ABAPO splitting, which is used in [6], to arrive at the numerical integrator

$$\psi^{\Delta t}_{ABAPO} = \exp\left(\frac{\Delta t}{2}\mathcal{L}_A\right)\exp(\Delta t\mathcal{L}_B)\exp\left(\frac{\Delta t}{2}\mathcal{L}_A\right)\exp(\Delta t\mathcal{L}_P)\exp(\Delta t\mathcal{L}_O), \tag{3.17}$$

where $\mathcal{L}_f$ is the corresponding operator for the vector field $f$. The phase ABA is the velocity Verlet algorithm.

GenKR PBCs are applied at the beginning of the scheme and after each integration in the position, in order to keep the particle inside the box. The ABAPO algorithm is described as follows:

**Algorithm 4** ABAPO

**for** $k \leftarrow 1 \dots$ Nsteps **do**
  $\textsc{GenKR}(\widetilde{\mathbf{q}}^k, \widetilde{\mathbf{p}}^k)$ ▷ Apply PBCs
  $\widetilde{\mathbf{p}}^{k+\frac{1}{4}} \leftarrow \widetilde{\mathbf{p}}^k + \frac{\Delta t}{2}\nabla E(\widetilde{\mathbf{q}}^k)$
  $\widetilde{\mathbf{q}}^{k+1} \leftarrow \widetilde{\mathbf{q}}^k + \frac{\Delta t}{2}\widetilde{\mathbf{p}}^{k+\frac{1}{4}}$
  $\textsc{GenKR}(\widetilde{\mathbf{p}}^{k+\frac{1}{4}}, \widetilde{\mathbf{q}}^{k+1})$
  $\widetilde{\mathbf{p}}^{k+\frac{1}{2}} \leftarrow \widetilde{\mathbf{p}}^{k+\frac{1}{4}} + \frac{\Delta t}{2}\nabla E(\widetilde{\mathbf{q}}^{k+1})$
  $\widetilde{\mathbf{p}}^{k+\frac{3}{4}} \leftarrow \exp(\Delta t A)\widetilde{\mathbf{p}}^{k+\frac{1}{2}}$
  $\widetilde{\mathbf{p}}^{k+1} \leftarrow \gamma\widetilde{\mathbf{p}}^{k+\frac{3}{4}} + (1-\gamma)A\widetilde{\mathbf{q}}^{k+1} + \sqrt{\beta^{-1}(1-\exp(-2\gamma\Delta t))}\boldsymbol{\zeta}^k$

In our numerical tests run, we observe a similar loss of order of convergence as in the SE-A case, as displayed in Figure 3.2. There doesn't seem to be a single observed rate of convergence, though it is clear that it is lower than first order.

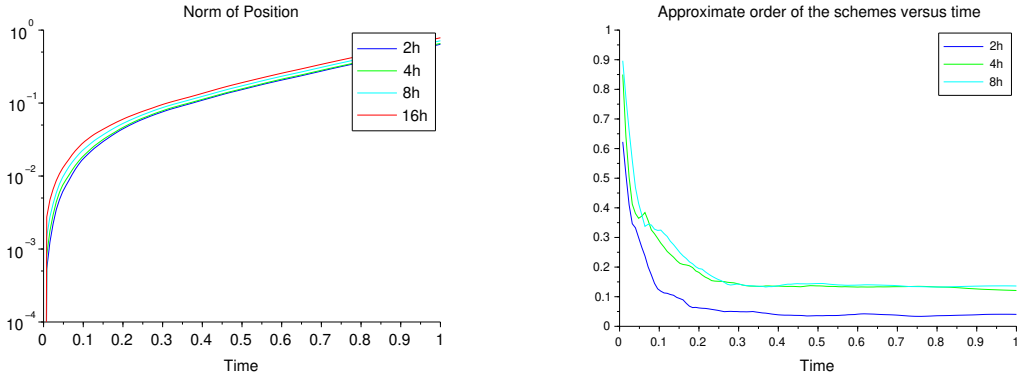


(a) (b)

**Figure 3.2:** (a) The strong error of the ABAPO scheme for decreasing step sizes is plotted as a function of time. (b) The estimated order of convergence, which is both irregular and less than the expected order $r = 1$. A corrected version of the scheme is presented in Section 3.6.

## 3.6 First Order NELD Algorithms

In this section, we will analyze four first order NELD integrators, two of which are corrected versions of Algorithms 3 and 4.

### 3.6.1 Euler-Maruyama

The Euler-Maruyama integrator for NELD differs from the SE-A algorithm above since we do not need to update the position before integrating the momentum, leading to only one application of the periodic boundary conditions. Thus we get the algorithm:

**Algorithm 5** Euler-Maruyama

**for** $k \leftarrow 1 \ldots$ Nsteps **do**
  GenKR($\widetilde{\mathbf{q}}^k, \widetilde{\mathbf{p}}^k$)
  $\widetilde{\mathbf{q}}^{k+1} \leftarrow \widetilde{\mathbf{q}}^k + \Delta t \widetilde{\mathbf{p}}^k$
  $\widetilde{\mathbf{p}}^{k+1} \leftarrow \widetilde{\mathbf{p}}^k + \Delta t \mathrm{F}(\widetilde{\mathbf{q}}^k, \widetilde{\mathbf{p}}^k) + \sigma \Delta t^{1/2} \boldsymbol{\xi}^k$

Writing the update rule, and taking into account the application of PBCs, we have

$$\begin{aligned}
\begin{bmatrix} \widetilde{\mathbf{q}}^{k+1} \\ \widetilde{\mathbf{p}}^{k+1} \end{bmatrix} &= \begin{bmatrix} \widetilde{\mathbf{q}}^k - L\mathbf{n} \\ \widetilde{\mathbf{p}}^k - AL\mathbf{n} \end{bmatrix} + \Delta t \begin{bmatrix} \widetilde{\mathbf{p}}^k - AL\mathbf{n} \\ \mathrm{F}(\widetilde{\mathbf{p}}^k - AL\mathbf{n}, \widetilde{\mathbf{q}}^k - L\mathbf{n}) \end{bmatrix} + \Delta t^{\frac{1}{2}} \begin{bmatrix} 0 & 0 \\ 0 & \sigma I \end{bmatrix} \boldsymbol{\xi}^k \\
&= \begin{bmatrix} \widetilde{\mathbf{q}}^k - L\mathbf{n} \\ \widetilde{\mathbf{p}}^k - AL\mathbf{n} \end{bmatrix} + \Delta t \begin{bmatrix} \widetilde{\mathbf{p}}^k - AL\mathbf{n} \\ \mathrm{F}(\widetilde{\mathbf{q}}^k, \widetilde{\mathbf{p}}^k) - A^2 L\mathbf{n} \end{bmatrix} + \Delta t^{\frac{1}{2}} \begin{bmatrix} 0 & 0 \\ 0 & \sigma I \end{bmatrix} \boldsymbol{\xi}^k.
\end{aligned}$$

Comparing with (3.12), we compute the leading orders of the local truncation error, finding $O(\Delta t^{\frac{3}{2}})$ stochastic terms and $O(\Delta t^2)$ deterministic terms,

$$T_2 = \frac{\Delta t^2}{2}\begin{bmatrix} \mathrm{F}(\widetilde{\mathbf{p}},\widetilde{\mathbf{q}}) \\ (-\nabla^2 E(\widetilde{\mathbf{q}}) + \gamma A)\widetilde{\mathbf{p}} + (A-\gamma I)\mathrm{F}(\widetilde{\mathbf{p}},\widetilde{\mathbf{q}}) \end{bmatrix} + \sigma\Delta t^{\frac{3}{2}} \begin{bmatrix} 0 & I \\ 0 & (A-\gamma I) \end{bmatrix} \left(\frac{1}{2}\boldsymbol{\xi}^k + \frac{1}{2\sqrt{3}}\boldsymbol{\eta}^k\right).$$

Therefore, the scheme will converge to the first order, which is confirmed numerically in Figure 3.3.

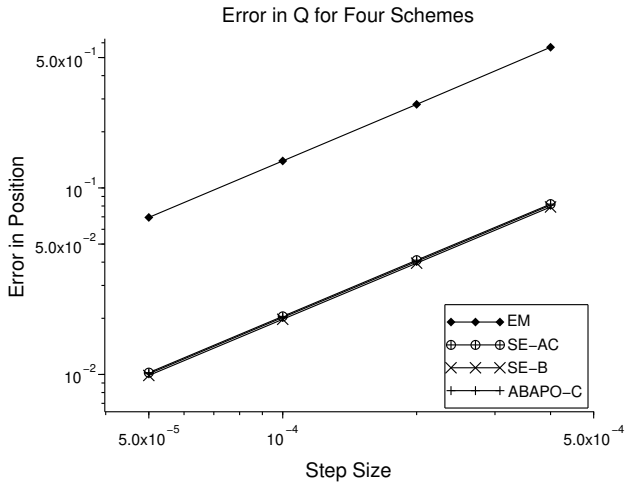


**Figure 3.3:** Four first-order convergent methods are plotted together, Euler-Maruyama (EM), corrected Symplectic Euler-A (SE-AC), Symplectic Euler-B (SE-B), and the corrected ABAPO splitting scheme (ABAPO-C). The schemes are compared against the second-order SOILE-A method, presented below, which is computed with stepsize $h = 2.5 \times 10^{-5}$. The error is averaged over 200 runs, where for a single run, the same Weiner process $W(t)$ is used for all the schemes.

### 3.6.2 Symplectic Euler B (SE-B)

In Symplectic Euler B, the momentum is integrated first, then the position. The periodic boundary conditions need only be applied a single time during the inner loop, and we have the following pseudocode:

**Algorithm 6** Symplectic Euler B

**for** $k \leftarrow 1 \ldots$ Nsteps **do**
  GenKR$(p, q)$
  $\widetilde{\mathbf{p}}^{k+1} \leftarrow \widetilde{\mathbf{p}}^{k} + \Delta t\ \mathrm{F}(\widetilde{\mathbf{p}}^{k+1}, \widetilde{\mathbf{q}}^{k}) + \Delta t^{\frac{1}{2}} \sigma \boldsymbol{\xi}^{k}$
  $\widetilde{\mathbf{q}}^{k+1} \leftarrow \widetilde{\mathbf{q}}^{k} + \Delta t\ \widetilde{\mathbf{p}}^{k+1}$

The numerical scheme is implicit in $\widetilde{\mathbf{p}}$, though it is linear in $\widetilde{\mathbf{p}}^{k+1}$, and a perturbation of the identity, so that we can solve for $\widetilde{\mathbf{p}}^{k+1}$ and expand in powers of $\Delta t$, to find

$$
\begin{aligned}
\begin{bmatrix} \widetilde{\mathbf{q}}^{k+1} \\ \widetilde{\mathbf{p}}^{k+1} \end{bmatrix} &= \begin{bmatrix} \widetilde{\mathbf{q}}^{k} - L\mathbf{n} \\ \widetilde{\mathbf{p}}^{k} - AL\mathbf{n} \end{bmatrix} \\
&\quad + \Delta t \begin{bmatrix} \widetilde{\mathbf{p}}^{k} - AL\mathbf{n} + \Delta t(\mathrm{F}(\widetilde{\mathbf{p}}^{k+1}, \widetilde{\mathbf{q}}^{k} - L\mathbf{n})) \\ \mathrm{F}(\widetilde{\mathbf{p}}^{k+1}, \widetilde{\mathbf{q}}^{k} - L\mathbf{n}) \end{bmatrix} + \sigma \Delta t^{\frac{1}{2}} \begin{bmatrix} 0 & 0 \\ 0 & \sigma I \end{bmatrix} \boldsymbol{\xi}^{k} \\
&= (I + (\gamma I - A)\Delta t)^{-1} \left( \begin{bmatrix} (I + (\gamma I - A)\Delta t)(\widetilde{\mathbf{q}}^{k} - L\mathbf{n}) \\ \widetilde{\mathbf{p}}^{k} - AL\mathbf{n} \end{bmatrix} \right. \\
&\quad + \Delta t \begin{bmatrix} \widetilde{\mathbf{p}}^{k} - AL\mathbf{n} + \Delta t(-\nabla E(\widetilde{\mathbf{q}}^{k}) + \gamma A(\widetilde{\mathbf{q}}^{k} - L\mathbf{n})) \\ (-\nabla E(\widetilde{\mathbf{q}}^{k}) + \gamma A(\widetilde{\mathbf{q}}^{k} - L\mathbf{n})) \end{bmatrix} \\
&\quad \left. + \sigma \Delta t^{\frac{1}{2}} \begin{bmatrix} 0 & 0 \\ 0 & I \end{bmatrix} \boldsymbol{\xi}^{k} \right) \\
&= \begin{bmatrix} \widetilde{\mathbf{q}}^{k} - L\mathbf{n} \\ \widetilde{\mathbf{p}}^{k} - AL\mathbf{n} \end{bmatrix} + \Delta t \begin{bmatrix} \widetilde{\mathbf{p}}^{k} - AL\mathbf{n} \\ \mathrm{F}(\widetilde{\mathbf{p}}^{k}, \widetilde{\mathbf{q}}^{k}) - A^2 L\mathbf{n} \end{bmatrix} \\
&\quad + \Delta t^2 \begin{bmatrix} \mathrm{F}(\widetilde{\mathbf{p}}^{k}, \widetilde{\mathbf{q}}^{k}) - A^2 L\mathbf{n} \\ (A - \gamma I)(\mathrm{F}(\widetilde{\mathbf{p}}^{k}, \widetilde{\mathbf{q}}^{k}) - A^2 L\mathbf{n}) \end{bmatrix} + \sigma \Delta t^{\frac{1}{2}} \begin{bmatrix} 0 & 0 \\ 0 & I \end{bmatrix} \boldsymbol{\xi}^{k} \\
&\quad + \sigma \Delta t^{\frac{3}{2}} \begin{bmatrix} 0 & I \\ 0 & (A - \gamma I) \end{bmatrix} \left( \frac{1}{2} \boldsymbol{\xi}^{k} + \frac{1}{2\sqrt{3}} \boldsymbol{\eta}^{k} \right) + O(\Delta t^{\frac{5}{2}}).
\end{aligned}
$$

As in the case of the Euler-Maruyama scheme, we find that the local truncation error is $O(\Delta t^{\frac{3}{2}})$ in the stochastic terms and $O(\Delta t^2)$ in the deterministic terms,

$$T_3 = \frac{\Delta t^2}{2}\begin{bmatrix} -\mathrm{F}(\widetilde{\mathbf{p}},\widetilde{\mathbf{q}}) \\ (-\nabla^2 E(\widetilde{\mathbf{q}}) + \gamma A)\widetilde{\mathbf{p}} - (A-\gamma I)\mathrm{F}(\widetilde{\mathbf{p}},\widetilde{\mathbf{q}}) \end{bmatrix} + \sigma\Delta t^{\frac{3}{2}}\begin{bmatrix} 0 & I \\ 0 & (A-\gamma I) \end{bmatrix}\left(\frac{1}{2}\boldsymbol{\xi}^k + \frac{1}{2\sqrt{3}}\boldsymbol{\eta}^k\right).$$

The global truncation error converges to the first order. The numerical results illustrated in Figure 3.3 confirm the analytical result.

### 3.6.3 Symplectic Euler A Corrected (SE-AC) and ABAPO Corrected (ABAPO-C)

The difference between ABAPO/SE-A and the corrected schemes ABAPO-C/SE-AC presented here resides in the fact that applying periodic boundary conditions is only done once during the scheme, while interparticle forces $-\nabla E(\widetilde{\mathbf{q}})$ are computed using the periodic conditions (while particles may rest outside the box). Thus we get algorithms 7 and 8 for SE-AC and ABAPO-C, respectively.

**Algorithm 7** Symplectic Euler A Corrected (SE-AC)

**for** $k \leftarrow 1 \ldots$ Nsteps **do**
  GenKR($\widetilde{\mathbf{q}}^k, \widetilde{\mathbf{p}}^k$)
  $\widetilde{\mathbf{q}}^{k+1} \leftarrow \widetilde{\mathbf{q}}^k + \Delta t\widetilde{\mathbf{p}}^k$
  $\widetilde{\mathbf{p}}^{k+1} \leftarrow \widetilde{\mathbf{p}}^k + \Delta t F_{\mathrm{PBC}}(\widetilde{\mathbf{p}}^k, \widetilde{\mathbf{q}}^{k+1}) + \sigma\Delta t^{\frac{1}{2}}\boldsymbol{\xi}^k$

**Algorithm 8** ABAPO-C

**for** $k \leftarrow 1 \dots$ Nsteps **do**
  GenKR($\widetilde{\mathbf{q}}^k, \widetilde{\mathbf{p}}^k$) ▷ Apply PBCs at the beginning of each iteration
  $\widetilde{\mathbf{p}}^{k+\frac{1}{4}} \leftarrow \widetilde{\mathbf{p}}^k + \frac{\Delta t}{2} \nabla V(\widetilde{\mathbf{q}}^k)$
  $\widetilde{\mathbf{q}}^{k+1} \leftarrow \widetilde{\mathbf{q}}^k + \frac{\Delta t}{2} \widetilde{\mathbf{p}}^{k+\frac{1}{4}}$
  $\widetilde{\mathbf{p}}^{k+\frac{1}{2}} \leftarrow \widetilde{\mathbf{p}}^{k+\frac{1}{4}} + \frac{\Delta t}{2} \nabla V_{\mathrm{PBC}}(\widetilde{\mathbf{q}}^{k+1})$
  $\widetilde{\mathbf{p}}^{k+\frac{3}{4}} \leftarrow \exp(\Delta t A) \widetilde{\mathbf{p}}^{k+\frac{1}{2}}$
  $\widetilde{\mathbf{p}}^{k+1} \leftarrow \gamma \widetilde{\mathbf{p}}^{k+\frac{3}{4}} + (1-\gamma) A \widetilde{\mathbf{q}}^{k+1} + \sigma \Delta t^{\frac{1}{2}} \boldsymbol{\xi}^k$

Expanding out SE-AC, we have a similar expression to SE-A (3.14), though there is only a single application of periodic boundary conditions, so we have

$$\begin{aligned}
\begin{bmatrix} \widetilde{\mathbf{q}}^{k+1} \\ \widetilde{\mathbf{p}}^{k+1} \end{bmatrix} &= \begin{bmatrix} \widetilde{\mathbf{q}}^k - L\mathbf{n} \\ \widetilde{\mathbf{p}}^k - AL\mathbf{n} \end{bmatrix} \\
&\quad + \Delta t \begin{bmatrix} \widetilde{\mathbf{p}}^k - AL\mathbf{n} \\ \mathrm{F}(\widetilde{\mathbf{p}}^k - AL\mathbf{n}, \widetilde{\mathbf{q}}^k - L\mathbf{n} + \Delta t(\widetilde{\mathbf{p}}^k - AL\mathbf{n})) \end{bmatrix} + \begin{bmatrix} 0 & 0 \\ 0 & \sigma I \end{bmatrix} \boldsymbol{\xi}^k \\
&= \begin{bmatrix} \widetilde{\mathbf{q}}^k - L\mathbf{n} \\ \widetilde{\mathbf{p}}^k - AL\mathbf{n} \end{bmatrix} + \Delta t \begin{bmatrix} \widetilde{\mathbf{p}}^k - AL\mathbf{n} \\ \mathrm{F}(\widetilde{\mathbf{q}}^k, \widetilde{\mathbf{p}}^k) - A^2 L\mathbf{n} \end{bmatrix} + \sigma \Delta t^{\frac{1}{2}} \begin{bmatrix} 0 & 0 \\ 0 & I \end{bmatrix} \boldsymbol{\xi}^k \\
&\quad + \Delta t^2 \begin{bmatrix} 0 \\ \gamma A(\widetilde{\mathbf{p}}^k - AL\mathbf{n}) - \nabla^2 E(\widetilde{\mathbf{q}}^k)(\widetilde{\mathbf{p}}^k - AL\mathbf{n}) \end{bmatrix}.
\end{aligned}$$

Then the leading order terms in the local truncation error are $O(\Delta t^{\frac{3}{2}})$ in the stochastic terms and $O(\Delta t^2)$ in the deterministic terms,

$$T_4 = \frac{\Delta t^2}{2}\begin{bmatrix} \mathrm{F}(\widetilde{\mathbf{p}},\widetilde{\mathbf{q}}) + A^2 L\mathbf{n} \\ (\nabla^2 E(\widetilde{\mathbf{q}}) - \gamma A)\,\widetilde{\mathbf{p}} + (A-\gamma I)\mathrm{F}(\widetilde{\mathbf{p}},\widetilde{\mathbf{q}}) \end{bmatrix} \tag{3.18}$$

$$+ \sigma\Delta t^{\frac{3}{2}} \begin{bmatrix} 0 & I \\ 0 & (A-\gamma I) \end{bmatrix} \left(\frac{1}{2}\boldsymbol{\xi}^k + \frac{1}{2\sqrt{3}}\boldsymbol{\eta}^k\right). \tag{3.19}$$

Therefore, we expect to find first order convergence for the scheme, which is precisely what we observe in Figure 3.3. We similarly see the same improvement in convergence for the ABAPO-C scheme.

## 3.7 Second Order NELD Algorithms

We base our second order NELD integrators on algorithms developed for equilibrium Langevin dynamics in [63]. Since we need to integrate the position first in both methods, we apply the ideas from the corrected algorithm where we wait to remap the particle positions until the end of the variable updates. The SOILE-A scheme is a generalization of the Langevin equation for velocity-Verlet algorithm as is given by:

**Algorithm 9** Second Order Integrator of the Langevin Equation A (SOILE-A)

**for** $k \leftarrow 1 \ldots$ Nsteps **do**
$\textsc{GenKR}(\widetilde{\mathbf{q}}^k, \widetilde{\mathbf{p}}^k)$
$\widetilde{\mathbf{q}}^{k+1} \leftarrow \widetilde{\mathbf{q}}^k + \Delta t\widetilde{\mathbf{p}}^k + \frac{\Delta t^2}{2}F(\ \widetilde{\mathbf{p}}^k,\ \widetilde{\mathbf{q}}^k\ ) + \Delta t^{\frac{3}{2}}(\frac{1}{2}\boldsymbol{\xi}^k + \frac{1}{2\sqrt{3}}\boldsymbol{\eta}^k)$
$\widetilde{\mathbf{p}}^{k+1} \leftarrow \widetilde{\mathbf{p}}^k + (F_{\mathrm{PBC}}(\ \widetilde{\mathbf{p}}^k,\ \widetilde{\mathbf{q}}^{k+1}\ ) + \frac{\Delta t^2}{2}F(\ \widetilde{\mathbf{p}}^k,\ \widetilde{\mathbf{q}}^k\ )) + \sigma\Delta t^{\frac{1}{2}}\boldsymbol{\xi}^k - \frac{\Delta t^2}{2}(\gamma I - A)(F(\ \widetilde{\mathbf{p}}^k,\ \widetilde{\mathbf{q}}^k\ ) + \sigma\Delta t^{\frac{3}{2}}(\frac{1}{2}\boldsymbol{\xi}^k + \frac{1}{2\sqrt{3}}\boldsymbol{\eta}^k))$

SOILE-B is a quasi-symplectic scheme and is described as follows:

**Algorithm 10** Second Order Integrator of the Langevin Equation B (SOILE-B)

**for** $k \leftarrow 1 \ldots$ Nsteps **do**
$\textsc{GenKR}(\widetilde{\mathbf{q}}^k, \widetilde{\mathbf{p}}^k)$
$\widetilde{\mathbf{p}}^{k+\frac{1}{2}} \leftarrow \widetilde{\mathbf{p}}^k + \frac{\Delta t}{2} F(\ \widetilde{\mathbf{p}}^k,\ \widetilde{\mathbf{q}}^k\ ) - \frac{1}{4}(\gamma I - A)\big[\frac{\Delta t^2}{2} F(\ \widetilde{\mathbf{p}}^k,\ \widetilde{\mathbf{q}}^k\ ) + \sigma \Delta t^{\frac{3}{2}} (\frac{1}{2}\boldsymbol{\xi}^k + \frac{1}{\sqrt{3}}\boldsymbol{\eta}^k)\big]$
$\widetilde{\mathbf{q}}^{k+1} \leftarrow \widetilde{\mathbf{q}}^k + \Delta t \widetilde{\mathbf{p}}^{k+\frac{1}{2}} + \sigma \Delta t^{\frac{3}{2}} \frac{1}{\sqrt{3}} \boldsymbol{\eta}^k$
$\widetilde{\mathbf{p}}^{k+1} \leftarrow \widetilde{\mathbf{p}}^{k+\frac{1}{2}} + \frac{\Delta t}{2} \tilde{F}_{\mathrm{PBC}}(\ \widetilde{\mathbf{p}}^{k+\frac{1}{2}},\ \widetilde{\mathbf{q}}^{k+1}\ ) + \frac{1}{2}\sigma \Delta t^{\frac{1}{2}} \boldsymbol{\xi}^k$
$- \frac{\Delta t^2}{8}(\gamma I - A)\big[\tilde{F}_{\mathrm{PBC}}(\ \widetilde{\mathbf{p}}^{k+\frac{1}{2}},\ \widetilde{\mathbf{q}}^{k+1}\ ) + \sigma \Delta t^{\frac{3}{2}} (\frac{1}{2}\boldsymbol{\xi}^k + \frac{1}{\sqrt{3}}\boldsymbol{\eta}^k)\big]$

We write out the SOILE-A scheme, and expand out to second order, giving

$$
\begin{aligned}
\begin{bmatrix} \widetilde{\mathbf{q}}^{k+1} \\ \widetilde{\mathbf{p}}^{k+1} \end{bmatrix} &= \begin{bmatrix} \widetilde{\mathbf{q}}^{k} - L\mathbf{n} \\ \widetilde{\mathbf{p}}^{k} - AL\mathbf{n} \end{bmatrix} \\
&+ \Delta t \begin{bmatrix} \widetilde{\mathbf{p}}^{k} - AL\mathbf{n} \\ \frac{1}{2}(-\nabla E(\widetilde{\mathbf{q}}^{k+1}) - \nabla E(\widetilde{\mathbf{q}}^{k}) + \gamma A(\widetilde{\mathbf{q}}^{k+1} + \widetilde{\mathbf{q}}^{k})) - (\gamma I - A)(\widetilde{\mathbf{p}}^{k} - AL\mathbf{n}) \end{bmatrix} \\
&+ \sigma \Delta t^{\frac{1}{2}} \begin{bmatrix} 0 & 0 \\ 0 & I \end{bmatrix} \boldsymbol{\xi}^{k} + \frac{\Delta t^{2}}{2} \begin{bmatrix} \mathrm{F}(\widetilde{\mathbf{q}}^{k}, \widetilde{\mathbf{p}}^{k}) - A^{2} L\mathbf{n} \\ 0 \end{bmatrix} \\
&+ \sigma \Delta t^{\frac{3}{2}} \begin{bmatrix} 0 & I \\ 0 & (A - \gamma I) \end{bmatrix} (\frac{1}{2}\boldsymbol{\eta}^{k} + \frac{1}{2\sqrt{3}}\boldsymbol{\xi}^{k}) \\
= \begin{bmatrix} \widetilde{\mathbf{q}}^{k} - L\mathbf{n} \\ \widetilde{\mathbf{p}}^{k} - AL\mathbf{n} \end{bmatrix} &+ \Delta t \begin{bmatrix} \widetilde{\mathbf{p}}^{k} - AL\mathbf{n} \\ \mathrm{F}(\widetilde{\mathbf{q}}^{k}, \widetilde{\mathbf{p}}^{k}) - A^{2} L\mathbf{n} \end{bmatrix} + \sigma \Delta t^{\frac{1}{2}} \begin{bmatrix} 0 & 0 \\ 0 & I \end{bmatrix} \boldsymbol{\xi}^{k} \\
&+ \frac{\Delta t^{2}}{2} \begin{bmatrix} \mathrm{F}(\widetilde{\mathbf{q}}^{k}, \widetilde{\mathbf{p}}^{k}) - A^{2} L\mathbf{n} \\ -(\nabla^{2} E(\widetilde{\mathbf{q}}^{k}) + \gamma A)(\widetilde{\mathbf{p}}^{k} - AL\mathbf{n}) + (A - \gamma I)(\mathrm{F}(\widetilde{\mathbf{q}}^{k}, \widetilde{\mathbf{p}}^{k}) - A^{2} L\mathbf{n}) \end{bmatrix} \\
&+ \sigma \Delta t^{\frac{3}{2}} \begin{bmatrix} 0 & I \\ 0 & (A - \gamma I) \end{bmatrix} \left( \frac{1}{2}\boldsymbol{\eta}^{k} + \frac{1}{2\sqrt{3}}\boldsymbol{\xi}^{k} \right) + O(\Delta t^{3}).
\end{aligned}
$$

These terms cancel with the exact expansion (3.12), with $O(\Delta t^{\frac{5}{2}})$ stochastic terms and $O(\Delta t^{3})$ deterministic terms, giving a globally second-order convergent scheme. We observe in Figure 3.4 exhibit second order convergence as predicted by the truncation error.

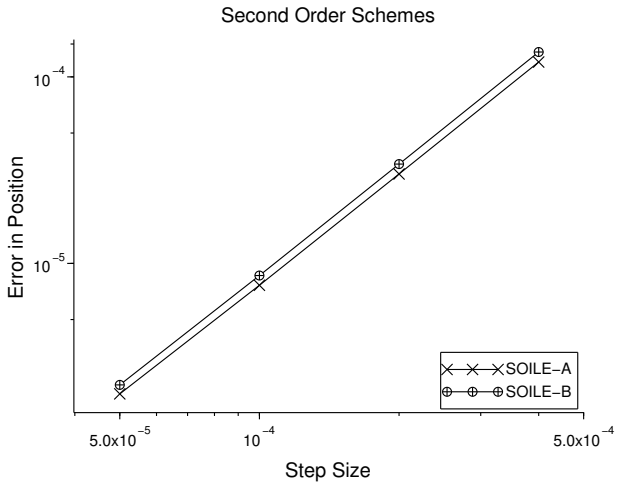


**Figure 3.4:** Estimated order of convergence for the SOILE-A and SOILE-B schemes. Both are observed to be second order, consistent with the truncation error analysis.

## 3.8 Conclusion

We have derived several numerical integrators for nonequilibrium Langevin dynamics and have shown that care must be taken in applying the periodic boundary conditions, or there can be a breakdown in the order of convergence. Provided that the periodic boundary conditions are not applied in the middle of an update step, we have demonstrated several prototypical schemes of order one and two applied to NELD. For these orders, deforming the domain is performed after all other updates, and we still achieve the desired accuracy.

Several extensions are possible. First, deriving conditions for general higher-order schemes that appropriately incorporate the deforming simulation box and nonequilibrium PBCs, for example, for general stochastic Runge-Kutta schemes or variational schemes will be of interest. Also, of large interest in molecular dynamics is the con-

vergence of the invariant measure of the numerical scheme to the invariant measure as in [6, 32]. The error between these two measures introduces a bias in computing long-time averages of the microscopic dynamics and is an important consideration for algorithm analysis. This is challenging in the present case, since unlike Langevin dynamics, there is not generally an analytic expression for the invariant measure of the original dynamics (3.1), and further work is needed to quantify this error and how it is affected by the deforming boundary conditions.

# BIBLIOGRAPHY


[1] Agarwal, U. S. Effect of initial conformation, flow strength, and hydrodynamic interaction on polymer molecules in extensional flows. *The Journal of Chemical Physics 113*, 8 (2000), 3397–3403.

[2] Artin, M. *Algebra*. Pearson Prentice Hall, 2011.

[3] Baranyai, András, and Cummings, Peter T. Steady state simulation of planar elongation flow by nonequilibrium molecular dynamics. *The Journal of Chemical Physics 110*, 1 (1999), 42–45.

[4] Bellet, Luc Rey. *Ergodic Properties of Markov Processes*. Springer Berlin Heidelberg, Berlin, Heidelberg, 2006, pp. 1–39.

[5] Bird, R. Byron, Curtiss, Charles F., Armstrong, Robert C., and Hassager, Ole. *Dynamics of Polymeric Liquids, Kinetic Theory (Dynamics of Polymer Liquids Vol. 2) (Volume 2)*, volume 2 ed. Wiley-Interscience, June 1987.

[6] Burrage, Kevin, and Lythe, Grant. Accurate stationary densities with partitioned numerical methods for stochastic differential equations. *SIAM Journal on Numerical Analysis 47*, 3 (2009), 1601–1618.

[7] Cancès, Eric, Legoll, Frédéric, and Stoltz, Gabriel. Theoretical and numerical comparison of some sampling methods for molecular dynamics. *ESAIM: M2AN 41*, 2 (2007), 351–389.

[8] Cass, Thomas, Crisan, Dan, Dobson, Paul, and Ottobre, Michela. Long-time behaviour of degenerate diffusions: UFG-type SDEs and time-inhomogeneous hypoelliptic processes. *Electronic Journal of Probability 26*, none (2021), 1 – 72.

[9] Daivis, P.J., Matin, M.L., and Todd, B.D. Nonlinear shear and elongational rheology of model polymer melts by non-equilibrium molecular dynamics. *Journal of Non-Newtonian Fluid Mechanics 111*, 1 (2003), 1 – 18.

[10] Dobson, Matthew. Periodic boundary conditions for long-time nonequilibrium molecular dynamics simulations of incompressible flows. *The Journal of Chemical Physics 141*, 18 (2014), 184103.

[11] Dobson, Matthew, and Geraldo, Abdel Kader. Strong convergence of integrators for nonequilibrium langevin dynamics. *Molecular Simulation 45*, 11 (2019), 912–920.

[12] Dobson, Matthew, and Geraldo, Abdel Kader. Convergence of nonequilibrium langevin dynamics for planar flows, 2022.

[13] Dobson, Matthew, and Geraldo, Abdel Kader A. Simple periodic boundary conditions for molecular simulation of uniaxial flow. *Journal of Computational Physics 473* (2023), 111740.

[14] Dobson, Matthew, Legoll, Frédéric, Lelièvre, Tony, and Stoltz, Gabriel. Derivation of langevin dynamics in a nonzero background flow field. *ESAIM: M2AN 47*, 6 (2013), 1583–1626.

[15] Ermak, Donald L., and McCammon, J. A. Brownian dynamics with hydrodynamic interactions. *The Journal of Chemical Physics 69*, 4 (1978), 1352–1360.

[16] Evans, Denis J., and Morriss, G. P. Nonlinear-response theory for steady planar couette flow. *Phys. Rev. A 30* (Sep 1984), 1528–1530.

[17] Evans, Denis J., and Morriss, Gary P. *Statistical mechanics of nonequilibrium liquids*. ANU E Press, Canberra, 2007.

[18] EWEN, J. P., HEYES, D. M., and DINI, D. Advances in nonequilibrium molecular dynamics simulations of lubricants and additives. *Friction 6*, 4 (2018), 349–386.

[19] Friedman, A. *Stochastic Differential Equations and Applications. Vol. 1*. Probability and mathematical statistics series, vol. 28. Academic Press, 1975.

[20] Hairer, Martin, and Mattingly, Jonathan. Yet another look at Harris' ergodic theorem for markov chains. *Seminar on Stochastic Analysis, Random Fields and Applications VI 63* (11 2008).

[21] Higham., Desmond J. An algorithmic introduction to numerical simulation of stochastic differential equations. *SIAM Review 43*, 3 (2001), 525–546.

[22] Hoover, William G., Ladd, Anthony J. C., and Moran, Bill. High-strain-rate plastic flow studied via nonequilibrium molecular dynamics. *Phys. Rev. Lett. 48* (Jun 1982), 1818–1820.

[23] Hörmander, L. The analysis of linear partial differential operators III: Pseudo-differential operators. *ZAMM - Journal of Applied Mathematics and Mechanics / Zeitschrift für Angewandte Mathematik und Mechanik 67*, 11 (1987), 579–579.

[24] Hunt, Thomas A. Periodic boundary conditions for the simulation of uniaxial extensional flow of arbitrary duration. *Molecular Simulation 42*, 5 (2016), 347–352.

[25] Jain, Aashish, Sasmal, Chandi, Hartkamp, Remco, Todd, B.D., and Prakash, J. Ravi. Brownian dynamics simulations of planar mixed flows of polymer solutions at finite concentrations. *Chemical Engineering Science 121* (2015), 245 – 257. 2013 Danckwerts Special Issue on Molecular Modelling in Chemical Engineering.

[26] Joubaud, R., Pavliotis, G. A., and Stoltz, G. Langevin dynamics with space-time periodic nonequilibrium forcing. *Journal of Statistical Physics 158* (2015), 1–36.

[27] Kloeden, P.E., and Platen, E. *Numerical Solution of Stochastic Differential Equations*. Springer-Verlag, 1992.

[28] Kraynik, A.M., and Reinelt, D.A. Extensional motions of spatially periodic lattices. *Int. J. Multiphase Flow 18*, 6 (1992), 1045 – 1059.

[29] Lang, Philipp S., Obermayer, Benedikt, and Frey, Erwin. Dynamics of a semi-flexible polymer or polymer ring in shear flow. *Phys. Rev. E 89* (Feb 2014), 022606.

[30] Lang, Serge. *Algebra*. Springer, New York, NY, 2002.

[31] Lees, A W, and Edwards, S F. The computer study of transport processes under extreme conditions. *J. Phys. C Solid State 5*, 15 (1972), 1921.

[32] Leimkuhler, Benedict, and Matthews, Charles. Rational construction of stochastic numerical methods for molecular sampling. *Applied Mathematics Research eXpress 2013*, 1 (2013), 34–56.

[33] Leimkuhler, Benedict, Matthews, Charles, and Stoltz, Gabriel. The computation of averages from equilibrium and nonequilibrium Langevin molecular dynamics. *IMA Journal of Numerical Analysis 36* (Jan. 2015), 13–79.

[34] Lelièvre, Tony, and Stoltz, Gabriel. Partial differential equations and stochastic methods in molecular dynamics. *Acta Numerica 25* (2016), 681–880.

[35] Lenstra, Arjen, Lenstra, H., and Lovász, László. Factoring polynomials with rational coefficients. *Mathematische Annalen 261* (12 1982).

[36] Li, Zhen, Xiong, Shiyun, Sievers, Charles, Hu, Yue, Fan, Zheyong, Wei, Ning, Bao, Hua, Chen, Shunda, Donadio, Davide, and Ala-Nissila, Tapio. Influence of thermostatting on nonequilibrium molecular dynamics simulations of heat conduction in solids. *The Journal of Chemical Physics 151*, 23 (2019), 234105.

[37] Mattingly, J.C., Stuart, A.M., and Higham, D.J. Ergodicity for SDEs and approximations: locally Lipschitz vector fields and degenerate noise. *Stochastic Processes and their Applications 101*, 2 (2002), 185–232.

[38] McPhie, M.G., Daivis, P.J., Snook, I.K., Ennis, J., and Evans, D.J. Generalized Langevin equation for nonequilibrium systems. *Physica A 299*, 3-4 (2001), 412–426.

[39] Mendelsohn, N. S. The equation $\phi(x) = k$. *Mathematics Magazine 49*, 1 (1976), 37–39.

[40] Menzel, A. G., Daivis, P. J., and Todd, B. D. Equilibrium and nonequilibrium molecular dynamics methods to compute the first normal stress coefficient of a model polymer solution. *Phys. Rev. Fluids 5* (Aug 2020), 084201.

[41] Meyn, Sean, and Tweedie, Richard. *Markov Chains and Stochastic Stability*, 2 ed. Cambridge Mathematical Library. Cambridge University Press, 2009.

[42] Meyn, Sean P., and Tweedie, R. L. Stability of Markovian processes III: Foster-Lyapunov criteria for continuous-time processes. *Advances in Applied Probability 25*, 3 (1993), 518–548.

[43] Neelov, Igor M., and Adolf, David B. Brownian dynamics simulations of dendrimers under elongational flow: bead rod model with hydrodynamic interactions. *Macromolecules 36*, 18 (2003), 6914–6924.

[44] Nicholson, David A., and Rutledge, Gregory C. Molecular simulation of flow-enhanced nucleation in n-eicosane melts under steady shear and uniaxial extension. *The Journal of Chemical Physics 145*, 24 (2016), 244903.

[45] Nishioka, Akihiro, Takahashi, Tatsuhiro, Masubuchi, Yuichi, Takimoto, Jun-ichi, and Koyama, Kiyohito. Description of uniaxial, biaxial, and planar elongational viscosities of polystyrene melt by the K-BKZ model. *Journal of Non-Newtonian Fluid Mechanics 89* (03 2000), 287–301.

[46] Niven, Ivan. *Irrational Numbers*, 1 ed., vol. 11. Mathematical Association of America, 1985.

[47] O'Connor, Thomas C., Alvarez, Nicolas J., and Robbins, Mark O. Relating chain conformations to extensional stress in entangled polymer melts. *Phys. Rev. Lett. 121* (Jul 2018), 047801.

[48] O'Connor, Thomas C., Ge, Ting, Rubinstein, Michael, and Grest, Gary S. Topological linking drives anomalous thickening of ring polymers in weak extensional flows. *Phys. Rev. Lett. 124* (Jan 2020), 027801.

[49] Oliveira, A. Sofia F., Ciccotti, Giovanni, Haider, Shozeb, and Mulholland, Adrian J. Dynamical nonequilibrium molecular dynamics reveals the structural basis for allostery and signal propagation in biomolecular systems. *The European Physical Journal B 94* (07 2021), 144.

[50] Öttinger, H. C. *Stochastic Processes in Polymeric Fluids*. Springer, 1996.

[51] Padding, J T, and Briels, W J. Systematic coarse-graining of the dynamics of entangled polymer melts: the road from chemistry to rheology. *Journal of Physics: Condensed Matter 23*, 23 (2011), 233101.

[52] Petravic, Janka, and Evans, Denis J. Approach to the non-equilibrium time-periodic state in a 'steady' shear flow model. *Molecular Physics 95*, 2 (1998), 219–231.

[53] Platen, E., Schurz, H., and Kloeden, P.E. *Numerical Solution of SDE Through Computer Experiments: Buch*. Springer Verlag, 1994.

[54] Snook, Ian. *The Langevin and Generalised Langevin Approach to the Dynamics of Atomic, Polymeric and Colloidal Systems*. Elsevier, Amsterdam, 2007.

[55] Stoltz, Chris, de Pablo, Juan, and D. Graham, Michael. Concentration dependence of shear and extensional rheology of polymer solutions: Brownian dynamics simulations. *Journal of Rheology 50* (03 2006), 137.

[56] Talay, D. Stochastic Hamiltonian systems: Exponential convergence to the invariant measure, and discretization by the implicit Euler scheme. *Markov Processes and Related Fields 8* (01 2002).

[57] Templeton, C., Elber, R., Ferrario, M., and Ciccotti, G. A new boundary driven nemd scheme for heat and particle diffusion in binary mixtures. *Molecular Physics 119*, 19-20 (2021), e1892849.

[58] Tierney, Luke. Markov Chains for Exploring Posterior Distributions. *The Annals of Statistics 22*, 4 (1994), 1701 – 1728.

[59] Todd, B. D., and Daivis, Peter J. Nonequilibrium molecular dynamics simulations of planar elongational flow with spatially and temporally periodic boundary conditions. *Phys. Rev. Lett. 81* (Aug 1998), 1118–1121.

[60] Todd, B. D., and Daivis, Peter J. The stability of nonequilibrium molecular dynamics simulations of elongational flows. *The Journal of Chemical Physics 112*, 1 (2000), 40–46.

[61] Todd, B.D., and Daivis, Peter J. A new algorithm for unrestricted duration nonequilibrium molecular dynamics simulations of planar elongational flow. *Comput. Phys. Commun. 117*, 3 (1999), 191 – 199.

[62] Todd, Billy D., and Daivis, Peter J. *Nonequilibrium Molecular Dynamics: Theory, Algorithms and Applications*. Cambridge University Press, 2017.

[63] Vanden-Eijnden, Eric, and Ciccotti, Giovanni. Second-order integrators for langevin equations with holonomic constraints. *Chemical Physics Letters 429*, 1-3 (9 2006), 310–316.

[64] Xu, Wen-Sheng, Carrillo, Jan-Michael Y., Lam, Christopher N., Sumpter, Bobby G., and Wang, Yangyang. Molecular dynamics investigation of the relaxation mechanism of entangled polymers after a large step deformation. *ACS Macro Letters 7*, 2 (2018), 190–195.